Environmental Science and Pollution Research (2022) 29:56178–56199
https://doi.org/10.1007/s11356-022-19641-w

RESEARCH ARTICLE

Ultrasonic assisted preparation of ultrafine Pd supported on NiFe-layered double hydroxides for p-nitrophenol degradation

Xuan Zhou[1] · Jiaming Shi[2] · Xuefeng Bai[1,2]

Received: 8 July 2021 / Accepted: 6 March 2022 / Published online: 25 March 2022

Abstract

NiFe-layered double hydroxide (NiFe-LDH)–loaded ultrafine Pd nanocatalysts (Pd/NiFe-LDHs) were prepared by a facile ultrasonic-assisted in situ reduction technology without any stabilizing agents or reducing agents. Pd/NiFe-LDHs were characterized by FT-IR, XRD, XPS, and TEM. PdNPs are uniformly dispersed on NiFe-LDHs with a particle size distribution of 0.77–2.06 nm and an average particle size of 1.43 nm. Hydroxyl groups in Fe–OH and Ni–OH were dissociated into hydrogen radicals (·H) excited by ultrasound, and ·H reduced Pd^{2+} to ultrafine PdNPs. Then, Pd was coordinated with O in Ni–O and Fe–O, which improved the stability of the catalysts. Pd/NiFe-LDHs completely degraded 4-NP in 5 min, and the TOF value was 597.66 h^{-1}, which was 16.7 times that of commercial Pd/C. The 4-NP conversion rate remained at 98.75% over Pd/NiFe-LDHs after 10 consecutive catalytic cycles. In addition, the catalyst also has high catalytic activity for the reduction of Congo red, methylene blue, and methyl orange by $NaBH_4$.

Keywords Ultrasonic-assisted reduction · NiFe layered double hydroxides · Ultrafine Pd nanocatalysts · Degradation of p-nitrophenol

Introduction

With the speedy development of the economy, environmental pollution is becoming increasingly serious (Bose 2010). Everything comes from water, so water resource pollution is the primary problem of environmental pollution (Zarei et al. 2020; Mahalakshmi et al. 2020). As industrial production wastewater flows into rivers and domestic wastewater flows into the ground, the ecological environment has been severely damaged, such as the disappearance of endangered species, the reduction of green area, and desertification of land (Walker et al. 2019). It has been found that there are a large number of heavy organic matters and metal ions in wastewater, which have great impacts on the survival of aquatic organisms and microbial degradation (Ge et al. 2021; Zhao et al. 2019; Allman et al. 2019; Hou et al. 2020). Nitroaromatic compounds are widely used in industrial production as intermediates in the manufacture of explosives, dyes, pesticides, pigments, drugs, rubber chemicals, wood preservatives, photographic chemicals, and fungicides (Moradi et al. 2020; Kose et al. 2019; Zhang et al. 2020; Abdelhamid 2021). Nitrophenols are important chemical raw materials; they account for a large proportion of organic pollutants (Al-Kahtani et al. 2018) and are highly toxic to humans and animals (Dai et al. 2020). They have good water solubility and are stable at room temperature; a small amount of inhalation will cause damage to the nervous system and even result in breathing difficulties and methemoglobinemia (Kubendhiran et al. 2018; Chu et al. 2019). Among them, p-nitrophenol (4-NP) has the strongest toxicity (Gupta et al. 2014). The degradation methods of 4-NP include the adsorption method (Liu et al. 2019, 2010), photodegradation method (Cipagauta-Diaz et al. 2019), and chemical catalytic degradation method (Liu and Zhao 2009; Cai et al. 2021). Chemical catalytic degradation has the advantages of high efficiency, small amount of reducing agent, and less restriction. More importantly, the catalyst can accelerate the degradation reaction of other pollutants at the same time; therefore, chemical methods

Responsible Editor: Philippe Garrigues

✉ Xuefeng Bai
tommybai@126.com

[1] Heilongjiang Academy of Sciences, Harbin, China

[2] School of Chemistry and Material Sciences, Heilongjiang University, Harbin 150080, China

are more widely used. In addition, its reduction product, p-aminophenol, is an important chemical raw material for the preparation of medicines (Zhang et al. 2011; Li et al. 2012) and is easily degraded and handled. The reduction of p-nitrophenol to p-aminophenol is an effective method to deal with this kind of pollutant.

In the chemical reduction method, the degradation of 4-NP by $NaBH_4$ is a typical reaction, and the key to this reaction is the development of high-efficiency catalysts. Wu et al. 2016 prepared a polyvinylidene fluoride (PVDF) membrane modified by AuNPs with a spacer (polydopamine), which can catalyze 4-NP degradation to reach more than 90% within 5 min (Riesz and Kondo 1992). Sun and his team successfully prepared a polycrystalline N-doped Cu/C/Cu_xO catalyst by N-coordinated cellulose, which improved the 4-NP degradation reaction rate (Sun et al. 2019). Naveen et al. prepared a Pt/porous SiO_2 hybrid structure catalyst, and its activity was significantly better than that of Ag and Au nanoparticle catalysts supported on SiO_2 (Bogireddy et al. 2020). Muhammad et al. used a two-step method to prepare porous polyurea microspheres (PPMs) and PdNP composite microspheres (Pd@PPM2), which have admirable catalytic stability and activity for degradation reactions of 4-NP and several dyes (Bashir et al. 2020). Liu et al. studied a Pd/TiO_2 catalyst for 3D printing hierarchical porous TiO_2 scaffolds modified with PdNPs (Liu et al.2020a, b). It can promote the rapid reduction of 4-NP wastewater at high concentrations and has good stability. In the catalytic 4-NP degradation reaction, Pd exhibits better catalytic activity and stability than other metals. In addition, Pd metal catalysts can also catalyze the degradation of other pollutants.

Veisi et al. (2020) prepared ultrafine PdNPs by in situ reduction on chitosan-coated Fe_3O_4/SiO_2-NH_2NPs (Veisi et al. 2020). The catalyst has good catalytic activity and stability for 4-NP degradation. Jaleh et al. used a liquid-phase laser ablation method to prepare a PdNP-modified C cloth (Jaleh et al. 2020). The catalyst has admirable catalytic stability and activity for the degradation of 4-NP and methylene blue. Liu et al. prepared a ZnO/Pd/PdO MF catalyst by calcining a precursor obtained by immersing three-dimensional ZnO microflowers (MFs) in a $PdCl_2$ ethanol solution in air (Liu et al. 2020a, b), and the catalyst had excellent catalytic activity for the degradation of 4-NP. PdNPs prepared by these methods have admirable adaptability activity and catalytic to degradation of 4-NP, but the preparation method of the carrier used in the catalyst is more complicated, which increases the production cost of the catalysts. The proper carrier is very important for the catalysts. Therefore, this study tried to select a cheap carrier with a facile preparation method, and the carrier was helpful for the formation of supported PdNPs with a smaller particle size, which showed better catalytic stability and activity for the degradation of p-nitrophenol.

Hydrotalcite, a kind of layered double hydroxide (LDH), is a hydroxide composed of divalent and trivalent metal ions (Gu et al. 2019), and the intercalation layer has a guest anion to adjust the charge. The number of layers, metal types, and layer spacing are adjustable. These characteristics make LDHs important in applications in different fields, such as catalysts, adsorbents, and sensors. (Abellán et al. 2014). Anantharaj et al. prepared a PdNP catalyst supported on NiFe-LDH crystal flakes by $NaBH_4$ with a hydrothermal method, which has good catalytic performance for OER (Anantharaj et al. 2017). Li et al. used polystyrene (PS) microspheres as a template to prepare a three-dimensional Ni–Fe-layered double hydroxide nanowire/nanoporous nickel intermediate layer/foamed nickel base electrocatalyst with two-step electrodeposition technology (Li et al. 2020a, b), which has desirable catalytic activity for OER. It can be seen that NiFe-LDHs are good carrier materials. Therefore, the performance of catalysts prepared with NiFe-LDHs as carriers on the degradation of 4-NP was studied. The surface of LDHs is rich in hydroxyl groups, similar to polyols. It has reducibility under external conditions and can reduce metal ions to metal nanoparticles. The chemical reaction of ultrasound in an aqueous solution is due to acoustic cavitation. The collapse, formation, and growth of bubbles contribute to abnormal chemical and physical effects that drive various chemical reactions to produce nanoparticles. Mohammadi et al. synthesized Ag-rGO nanocomposites by diethylene glycol with an ultrasonic-assisted reduction method to form smaller AgNPs (Mohammadi and Entezari 2018), which have good catalytic activity for the 4-NP degradation reaction. Nemamcha et al. successfully reduced Pd(II) nitrate in glycol and polyvinylpyrrolidone (PVP) solution by an ultrasonic-assisted method to obtain stable metal Pd (Nemamcha et al. 2006). Riesz et al. discussed the evidence that pulsed ultrasound forms free radicals in aqueous solutions and reviewed the role of free radicals and ultrasound-induced mechanical effects in DNA degradation, enzyme inactivation, lipid peroxidation, and cell killing (Riesz and Kondo 1992). Gültekin et al. carried out the laboratory reduction of azo dyes by ozone and ultrasonic methods (Gültekin and Ince 2006). Studies have shown that ozone transfer increases in solution and decomposes to produce ·OH and other oxidizing substances in the gas phase. Dunn et al. studied the role of water in the ultrasonic conversion process and provided more information for the conversion process of asphaltenes into gaseous oil and resin fractions under the action of cavitation and surfactants (Dunn and Yen

2001). In the ultrasound-assisted method, ultrasound can change the reaction path so that Ni–OH and Fe–OH are dissociated into ·H. This has been confirmed in previous studies by our group. Li et al. reduced Pd^{2+} to ultrafine PdNPs by hydrogen radicals from surface hydroxy groups on MgAl-LDHs excited by ultrasound, which has high activity in catalyzing the Suzuki reaction (Li, Bai et al. 2020). This provides an easy and green preparation method for metal nanoparticles without adding reducing agents and stabilizing agents.

The layered structure of NiFe-LDHs used in this study is rich in hydroxyl groups, and the large number of pores in NiFe-LDHs increases the specific surface area, making it extremely adsorbent (Lu et al. 2016) and having superior catalytic performance (Fang et al. 2021; Wang et al. 2021; Zhou et al. 2014). It can adsorb Pd^{2+} in aqueous solution and react with the ·H generated by the surface hydroxyl groups of NiFe-LDHs under the action of ultrasound. We tried to reduce Pd^{2+} to PdNPs to obtain PdNPs/NiFe-LDHs without an additional reducing agent and stabilizing agent and investigated the effect of the preparation conditions on their performance. The performance of Pd/NiFe-LDHs was studied by the reaction of 4-NP with $NaBH_4$. Furthermore, the catalytic adaptability for the reduction of CR, MB, and MO was also investigated.

Experimental

Preparation of supported catalyst

(1) Preparation of NiFe-LDHs

A 20-mL solution containing 15 mM $Ni(NO_3)_2$ and 5 mM $Fe(NO_3)_3$ was prepared as solution A, and then a 40-mL solution with 1 mol/L NaOH was prepared as solution B. Another 12.5-mL solution with 0.8 M Na_2CO_3 was prepared as solution C. Both solution A and solution B were added dropwise to solution C at a uniform speed at the same time. The obtained coprecipitation solution was placed in a closed container and crystallized for 18 h at 60 °C. Finally, NiFe-LDHs were obtained by centrifugation, washed to neutrality, and dried at 60 °C.

(2) Preparation of Pd/NiFe-LDHs

First, NiFe-LDHs (0.05 g) were dispersed with 15 mL of deionized water and sonicated at 400 W and 30 °C for 20 min to fully disperse them in the aqueous solution. Second, Na_2PdCl_4 (2.5 mL 0.01 M) was added to the aqueous solution and well mixed. Finally, the solution was sonicated at 400 W and 30 °C for 1 h and centrifuged to obtain the sample, named Pd/NiFe-LDHs.

(3) Preparation of the contrastive catalyst

Pd/NiFe-LDH-C was prepared by a chemical reduction method for comparison experiments. NiFe-LDHs (0.05 g) were dispersed with 15 mL of deionized water and then sonicated at 400 W and 30 °C for 20 min to fully disperse them in an aqueous solution, Na_2PdCl_4 (2.5 mL, 0.01 M) and $NaBH_4$ (5 mL, 0.01 M) solution were added to the aqueous solution to react at 30 °C for 1 h. Pd/NiFe-LDHs-C was obtained by centrifugation, washing, and drying.

Because the structure of NiFe-LDHs will be destroyed during the reduction of Pd^{2+} by H_2 under high-temperature conditions, the contrastive catalyst is only prepared by the method of $NaBH_4$ reduction.

4-NP degradation reaction catalyzed by Pd/NiFe-LDHs

The prepared $NaBH_4$ (0.01 M, 0.4 mL) and p-nitrophenol (0.06 mL, 0.01 M) solution was added to the cuvette, and deionized water was added to make the final solution volume consistent. After adding Pd/NiFe-LDHs, the solution gradually changed from light yellow to colorless, and the reaction course was evaluated by UV–Vis spectroscopy.

Kinetic calculation

The catalytic reduction mechanism of 4-NP follows the Langmuir–Hinshelwood mechanism (Wunder et al. 2010). Since the initial concentration is much greater than 4-NP, the quasi-first order kinetics can be used to estimate hydrogenation reduction. The apparent rate constant (k_a) of 4-NP reduction is calculated by the following formula:

$$\ln(C_t/C_0) = \ln(A_t/A_0) = k_a t$$

The conversion rate (CR) of the reaction is shown in the following formula:

$$CR = \frac{C_0 - C_t}{C_0} \times 100\% = \frac{A_0 - A_t}{A_0} \times 100\%$$

C_0 and C_t are the initial concentration and t (min) concentration for a certain time, respectively, and A_0 and A_t are the ultraviolet–visible absorbance at 0 min and t min, respectively.

To compare the catalytic performance of Pd/NiFe-LDHs with other reported catalysts, the normalized ratio constant is calculated as follows:

$$k_n = k_a/m$$

m (mg) is the mass of Pd in the catalyst.

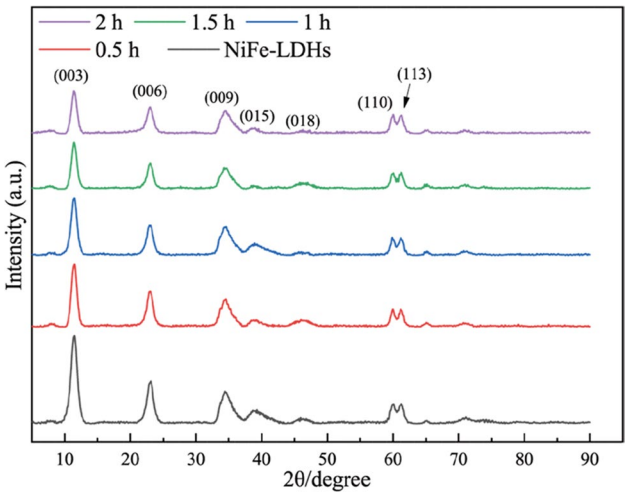

Fig. 1 XRD pattern of Pd/NiFe-LDHs prepared with different ultrasonic times

Table 1 Lattice parameters of Pd/NiFe-LDHs prepared at different ultrasonic times

Samples	d(003)/Å	d(110)/Å	d(113)/Å
NiFe-LDHs	7.77	1.54	1.51
NiFe-LDHs-0.5 h	7.76	1.54	1.51
NiFe-LDHs-1 h	7.75	1.54	1.51
NiFe-LDHs-1.5 h	7.71	1.54	1.51
NiFe-LDHs-2 h	7.70	1.54	1.51

The conversion rate (TOF) can quantitatively reflect the catalytic activity. The calculation formula of TOF is shown as follows:

$$TOF = \frac{n_0 \cdot CR}{t_c n_{cat}}$$

n_0 is the initial number of moles of 4-NP, CR is the conversion rate, t_c is the time required for the reaction, and n_{cat} is the number of moles of PdNPs in the catalyzed reaction.

The effect of preparation conditions on catalytic performance

The influence of ultrasonic time

In this study, Pd/NiFe-LDHs were obtained by ultrasonic-assisted reduction. The effects of ultrasonic time (0.5, 1, 1.5, 2 h) on the structure, morphology, and composition of the catalyst and the performance of the catalytic 4-NP reaction were investigated under the conditions of 400 W, 30 °C, and a Pd loading of 5 wt.%.

To understand the impact of ultrasound time on the structure of Pd/NiFe-LDHs, XRD analysis was implemented. The results are in Fig. 1 and Table 1.

From Fig. 1, the characteristic peaks of NiFe-LDHs appear at 2θ = 11°, 23°, 35°, 39°, and 47°, ascribed to the (003), (006), (009), (015), and (018) crystal planes, in accord with the LDH phase (JCPDS 22–700) (Tang et al. 2018; Hu et al. 2020). The double peaks at 2θ values of 60° and 61°were ascribed to the (110) and (113) crystal planes, which indicated that regular layered NiFe-LDH crystals had been formed. With the prolongation of ultrasonic time, the intensity of the peak of the (003) crystal plane became weaker, but the diffraction peaks of the (110) and (113) crystal

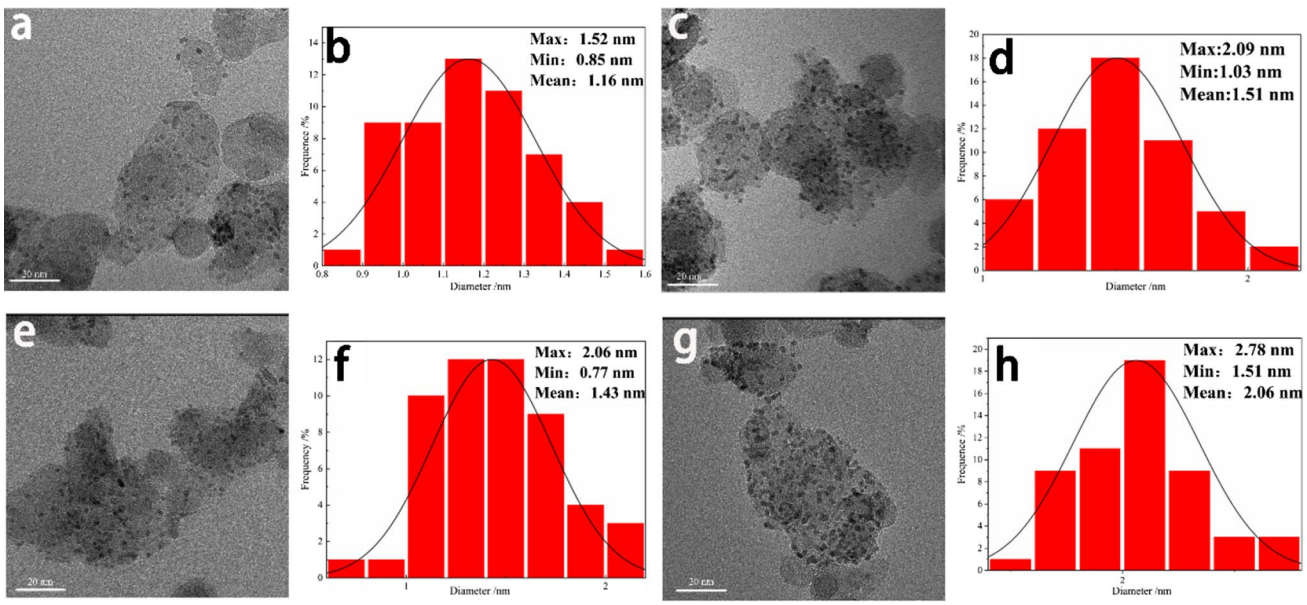

Fig. 2 TEM images and size distribution of Pd/NiFe-LDHs prepared at different ultrasonic times: 0.5 (**a**–**b**), 1 (**c**–**d**), 1.5 (**e**–**f**), 2 h (**g**–**h**)

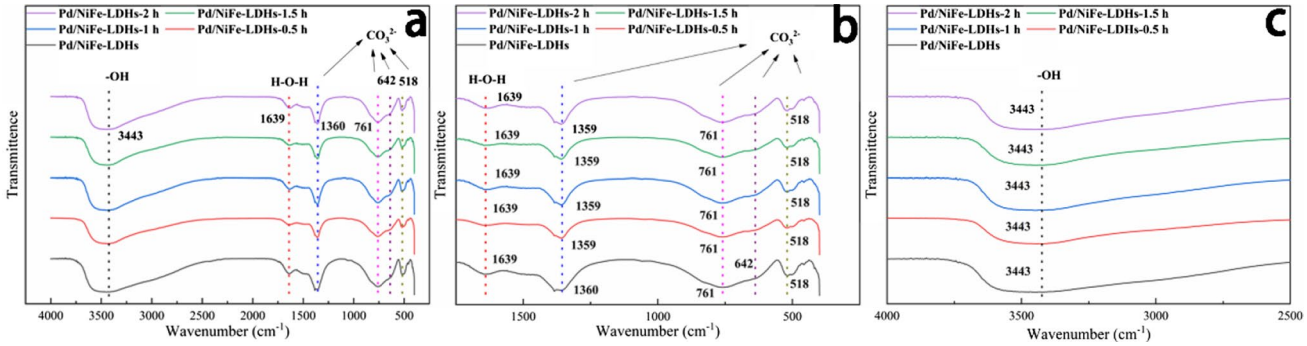

Fig. 3 FT-IR spectra of Pd/NiFe-LDHs prepared at different ultrasonic times: 4000–425 (**a**), 1750–425 (**b**), and 4000–2500 cm^{-1} (**c**)

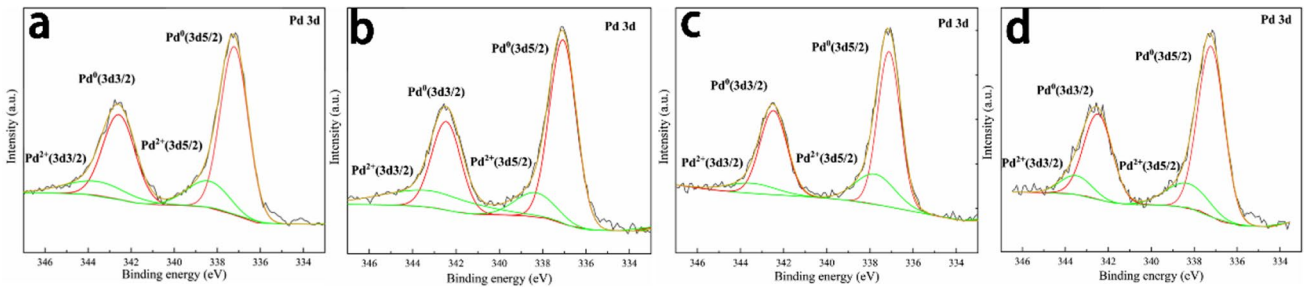

Fig. 4 XPS spectra of Pd 3d catalysts with different ultrasound times: 0.5 h (**a**), 1 h (**b**), 1.5 h (**c**), 2 h (**d**)

Table 2 Characteristic peak changes of each element

Ultrasonic time	Pd^0 $3d_{5/2}$	Pd^0 $3d_{3/2}$	Pd^{2+} $3d_{5/2}$	Pd^{2+} $3d_{3/2}$	Ni–OH	Ni^{2+}	Fe–OH	Fe^{3+}
0.5 h	337.06	342.45	338.35	343.25	856.09	861.89	712.39	715.46
1 h	337.15	342.45	338.34	343.33	855.80	861.53	712.32	715.36
1.5 h	337.21	342.47	338.35	343.51	855.78	861.44	712.30	715.37
2 h	337.21	342.47	338.34	343.65	855.78	861.44	712.24	715.11

planes had no obvious change, which indicated that ultrasound has no obvious effect on the layered structure of NiFe-LDHs and only changed the layer spacing. The results showed that the layered NiFe-LDHs were partially stripped, which was beneficial to the mass transfer process between the substrate and the catalytically active site and improved its catalytic activity. No Pd diffraction peaks were found at 2θ values of 47° and 40°, which were caused by two reasons. First, the small particle size, high dispersion, and low loading of PdNPs made the PdNP diffraction peaks weaker. Second, the diffraction peaks of the (111) and (200) crystal planes of Pd overlap with the diffraction peaks of the (015) and (018) crystal planes of NiFe-LDHs, respectively (Gursky et al. 2006; Liu and Yang 2016), which resulted in the covering of the diffraction peaks of PdNPs.

The influence of ultrasound time on the morphology of Pd nanoparticles on the surface of Pd/NiFe-LDHs was observed by TEM. The results are in Fig. 2.

From Fig. 2b, when the ultrasound time was 0.5 h, the PdNP particle size was the smallest, only 1.16 nm, but the small number of PdNPs indicated that Pd^{2+} could not be reduced completely. In Fig. 2(c, e, g), PdNPs were even spread on the surface of NiFe-LDHs, and the number of PdNPs increased. From Fig. 2d, when the ultrasound time was 1 h, the average particle size of PdNPs was 1.43 nm. Figure 2(f, h) shows that as the ultrasound time was extended, the average particle size increased accordingly: 2.08 nm in 1.5 h and 2.06 nm in 2 h were roughly similar. Therefore, the PdNPs prepared by the ultrasound-assisted method have good dispersibility, and as the ultrasound time increases, the average particle size of PdNPs first increases and then remains unchanged.

Table 3 The proportion of characteristic peaks of each element changes with time

Ultrasonic time	Pd^0	Pd^{2+}	Ni–OH	Ni^{2+}	Fe–OH	Fe^{3+}	Surface hydroxyl	Metal oxygen bond
0.5 h	75.20%	24.80%	53.25%	46.75%	61.26%	38.74%	83.83%	14.09%
1 h	78.78%	21.22%	51.14%	48.86%	60.30%	39.70%	82.55%	14.17%
1.5 h	81.03%	18.97%	50.41%	49.59%	57.98%	42.02%	81.76%	14.40%
2 h	83.42%	16.58%	49.47%	50.53%	56.35%	43.65%	80.39%	17.16%

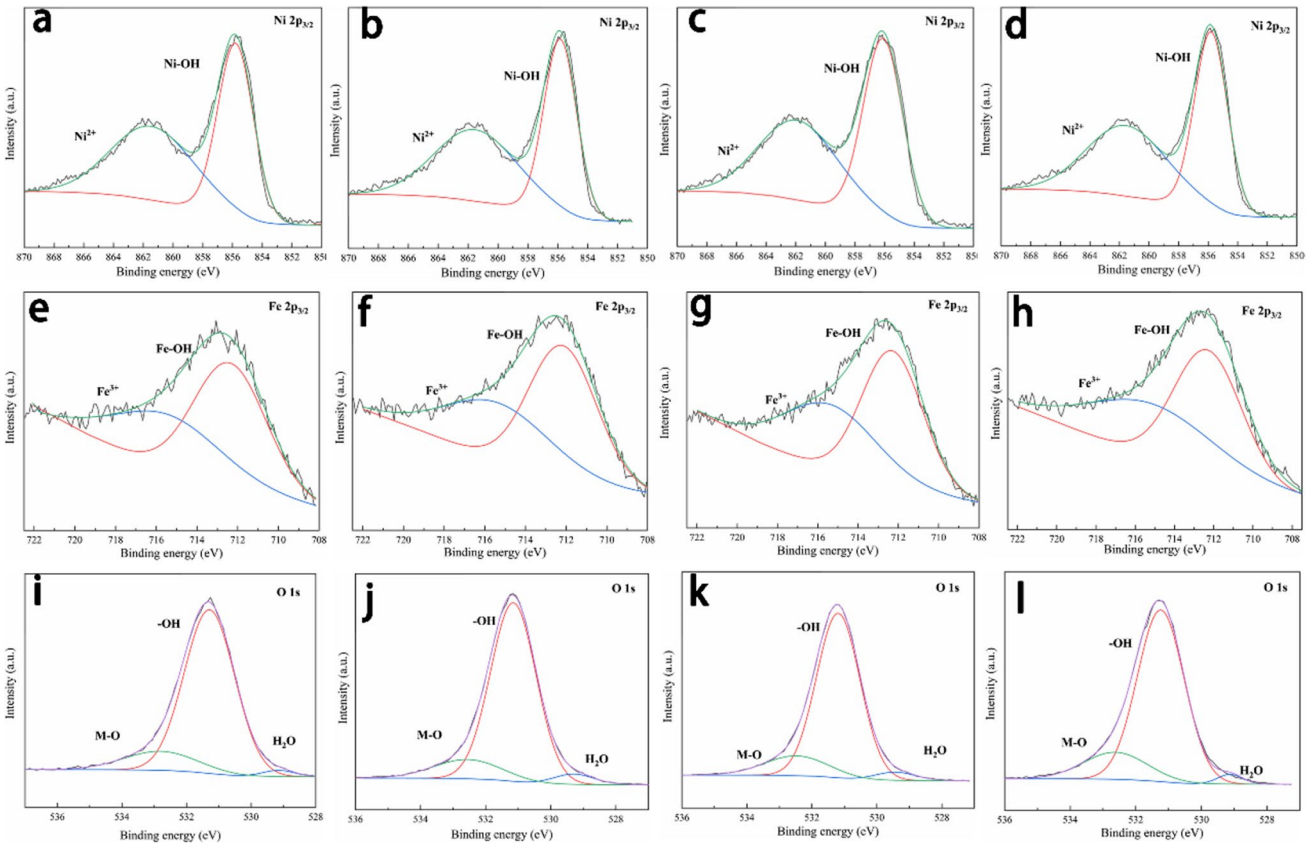

Fig. 5 XPS spectra of Ni 2p catalysts with different ultrasonic time: 0.5 (**a**), 1 (**b**), 1.5 (**c**), 2 h (**d**); XPS spectra of Fe 2p: 0.5 (**e**), 1 (**f**), 1.5 (**g**), 2 h (**h**); XPS spectra of O 1 s: 0.5 (**i**), 1 (**j**), 1.5 (**k**), 2 h (**l**)

To study the changes in NiFe-LDH surface functional groups with ultrasonic time, the prepared Pd/NiFe-LDHs were analyzed by FT-IR, and the results are in Fig. 3.

From Fig. 3a, the absorption peak at 3443 cm^{-1} was assigned to the expansion and deformation vibration peaks of -OH (Tang et al. 2018), and that at 1639 cm^{-1} was attributable to the expansion and deformation vibration peaks of water molecules. The peaks at 1360 cm^{-1} and 642 cm^{-1} were assigned to the v3 and v4 vibration peaks of CO_3^{2-}, and those at 761 cm^{-1} and 518 cm^{-1} corresponded to the interaction peaks of CO_3^{2-} and NiFe-LDHs (Wang et al. 2013). With prolonged ultrasound time, the intensity of the peaks (518 cm^{-1}, 3443 cm^{-1}) became weaker, which indicated that the content of CO_3^{2-} and -OH decreased, but the positions of the two peaks did not change significantly, which indicated that the ultrasonic time did not damage the layered structure of NiFe-LDHs.

To understand the effect of ultrasonic time on the valence state of Pd on the surface of Pd/NiFe-LDHs, XPS analysis was implemented on the prepared catalyst. The results are in Fig. 4.

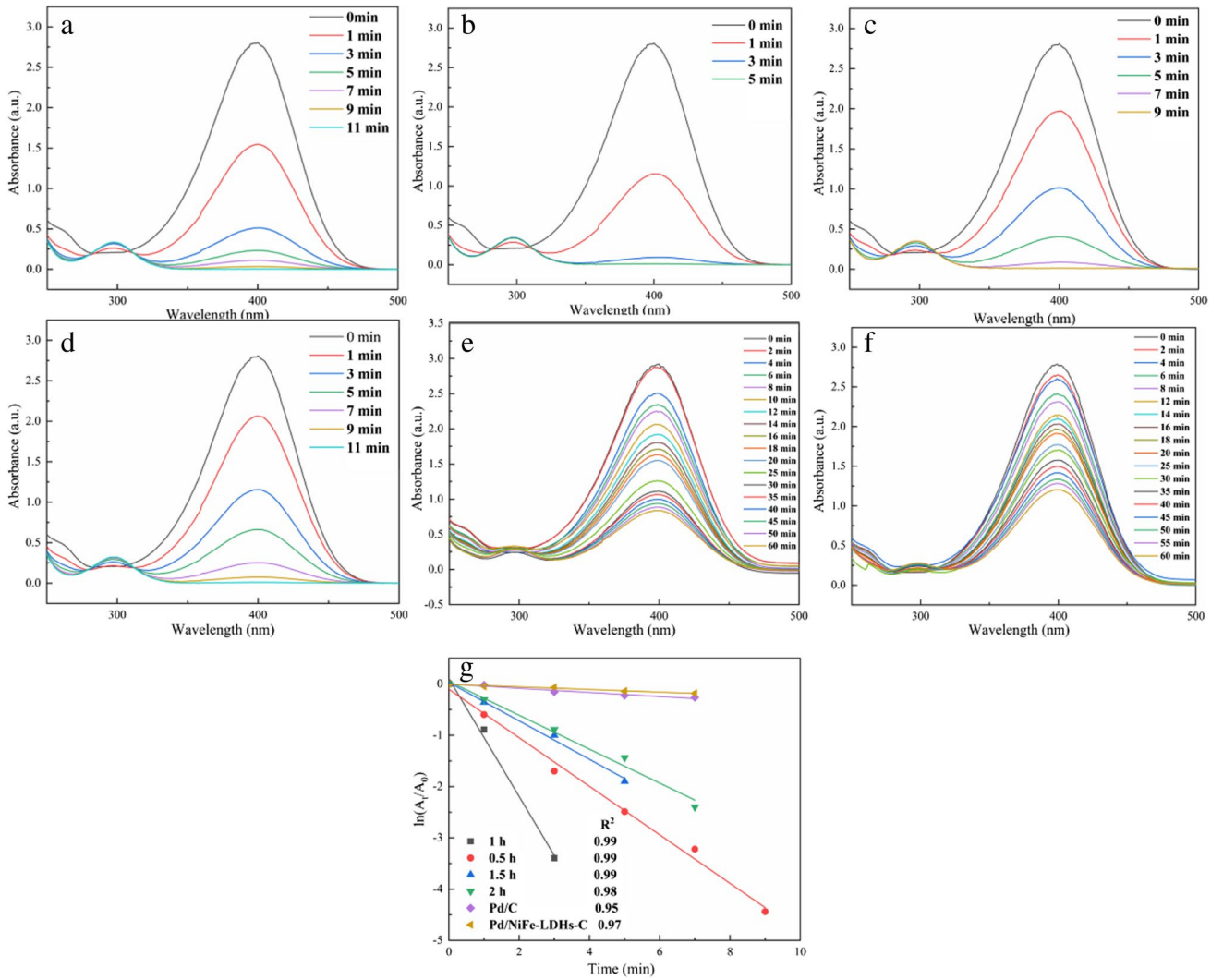

Fig. 6 The effect of ultrasound time on catalytic 4-NP degradation performance over Pd/NiFe-LDHs: 0.5 (**a**), 1 (**b**), 1.5 (**c**), 2 h (**d**), Pd/C (**e**), Pd/NiFe-LDHs-C (**f**), diagram of $\ln(A_t/A_0)$ against reaction time for catalysts prepared with different ultrasonic times and diagram of $\ln(A_t/A_0)$ against time for Pd/C and Pd/NiFe-LDHs-C (**g**)

Figure 4 shows that the binding energies (337.2 eV and 342.5 eV) could be regarded as characteristic peaks of Pd^0, and the binding energies of 338.4 eV and 343.5 eV could be regarded as characteristic peaks of Pd^{2+}. Compared with the standard Pd 3d (Pd $3d_{5/2}$: 335.4, 337.5 eV, Pd $3d_{3/2}$: 340.7, 342.3 eV) (Vafaeian et al., 2013; Rahmani et al. 2014), it was seen from Fig. 4 and Table 2 that with prolonged ultrasound time, the XPS characteristic peaks of Pd 3d gradually shifted to a high binding energy. The characteristic peaks of Fe 2p and Ni 2p gradually shifted to a low binding energy. Therefore, in the process of ultrasonic preparation, Pd interacted with Ni and Fe through O in Fe–OH and Ni–OH groups on the surface of NiFe-LDHs (Zhou et al. 2018), which shifted the characteristic peak

Table 4 Comparison of CR, k_n, TOF values, and k_a of different catalysts

Catalysts	wt.%	T_c/min	k_a/min^{-1}	k_n/mg^{-1} min^{-1}	CR/%	TOF/ h^{-1}
Pd/NiFe-LDHs-0.5 h	5	11	0.47	19.58	99.96	272.62
Pd/NiFe-LDHs-1 h	5	5	1.147	47.79	99.61	597.66
Pd/NiFe-LDHs-1.5 h	5	9	0.37	15.42	99.57	331.90
Pd/NiFe-LDHs-2 h	5	11	0.33	13.75	99.64	271.75
Pd/NiFe-LDHs-C	5	60	0.023	0.96	56.62	28.31
Pd/C-5%	5	60	0.036	1.5	71.37	35.69

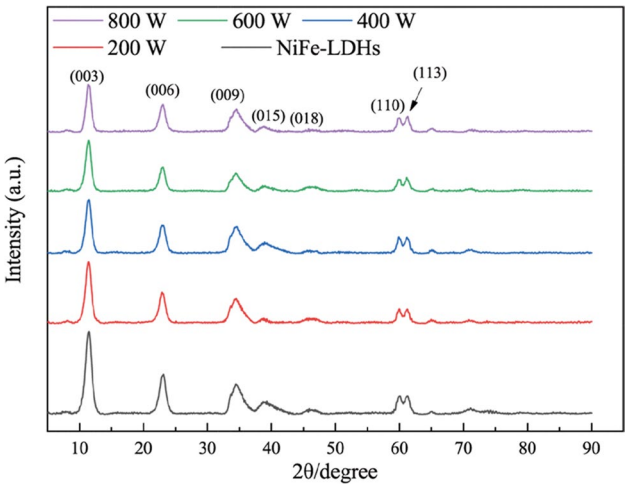

Fig. 7 XRD pattern of Pd/NiFe-LDHs prepared at different powers

of Pd 3d to the position of high binding energy. A large amount of -OH groups on the surface of LDHs attracted the electron cloud of Pd, which also increased the binding energy of Pd 3d (Liang et al. 2020). From Table 3, it can be seen that as the ultrasound time increased, the proportion of Pd^0 gradually increased, which indicated that Pd^{2+} was gradually reduced to Pd^0.

Table 5 The lattice parameters of Pd/NiFe-LDHs obtained at different ultrasonic power

Samples	d(003)/Å	d(110)/Å	d(113)/Å
NiFe-LDHs	7.77	1.54	1.51
NiFe-LDHs-200 W	7.77	1.54	1.51
NiFe-LDHs-400 W	7.75	1.54	1.51
NiFe-LDHs-600 W	7.74	1.54	1.51
NiFe-LDHs-800 W	7.74	1.54	1.51

To understand the changes in the composition and valence state of Ni, Fe, and O on the surface of Pd/NiFe-LDHs, XPS analysis was performed on the catalysts prepared at different ultrasonic times. The results are in Fig. 5.

From Fig. 5, Ni $2p_{3/2}$ could be divided into two peaks at 855.8 eV and 861.5 eV (Ni $2p_{3/2}$ binding energy position of standard NiFe-LDHs: 855.5 eV and 861.4 eV) (Gu et al. 2019), which were assigned to the characteristic peak of the Ni–OH bond and the satellite peak of Ni^{2+} in NiFe-LDHs, respectively. Fe $2p_{3/2}$ can also be divided into two peaks at 712.3 eV and 715.4 eV (Fe $2p_{3/2}$ binding energy position of standard NiFe-LDHs: 712.7 eV and 715.3 eV) (Wang et al. 2018; Ledendecker et al. 2015), assigned to characteristic peaks of Fe–OH bonds and satellite peaks of Fe^{3+}. From Table 2, the XPS characteristic peaks of Fe 2p and Ni 2p gradually shifted to a low binding energy with prolonged ultrasound time, which indicated that the interaction between Pd with Fe and Ni gradually increased. It can be seen from Table 3 that the proportion of the characteristic peaks of Fe–OH decreased with the ultrasound time, which shows that ultrasound made Ni–OH and Fe–OH change into ·H to reduce Pd^{2+}, and at the same time, Pd was coordinated with O in Fe–O and Ni–O. This reduced the proportion of characteristic peaks of Ni–OH and Fe–OH. O1 s can be divided into three peaks at 529.3 eV, 531.2 eV, and 532.5 eV, which are assigned to the characteristic peaks of adsorbed water molecules, hydroxyl groups, and metal oxygen bonds, respectively. As

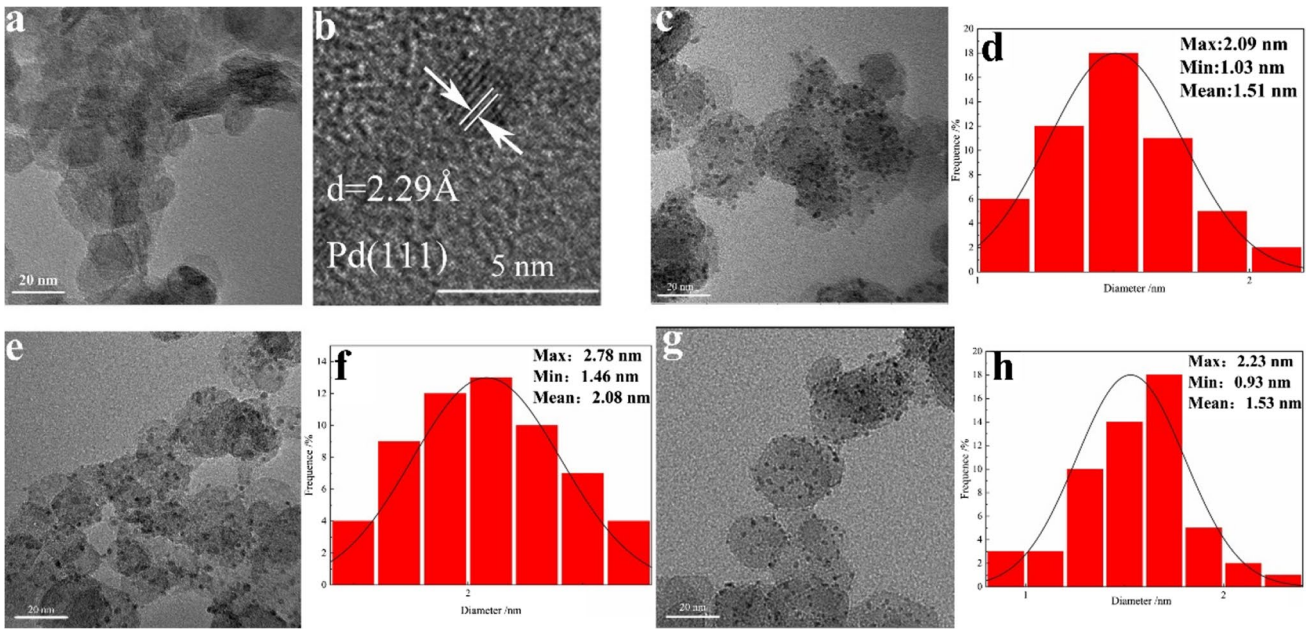

Fig. 8 TEM image and particle size distribution of Pd/NiFe-LDHs prepared with different ultrasonic power: 200 W (**a**), lattice fringes (**b**), 400 W (**c**–**d**), 600 W (**e**–**f**), 800 W (**g**–**h**)

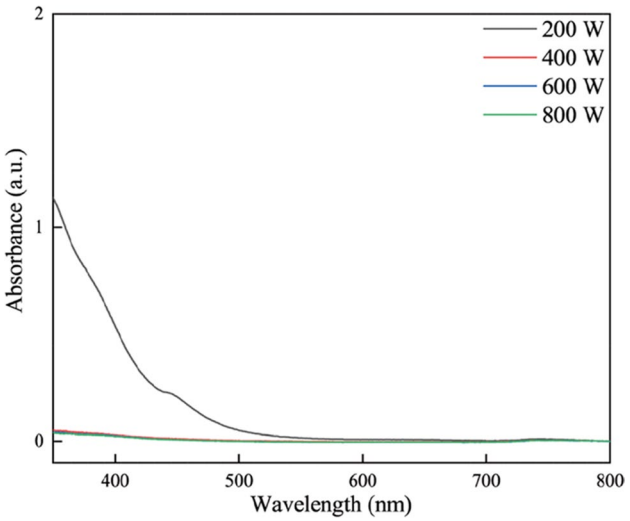

Fig. 9 UV–vis images of Pd/NiFe-LDHs supernatant prepared with different power

the ultrasound time increased, the proportion of the hydroxyl peak of 531.2 eV decreased, while the metal oxygen bond peak increased. It can be seen from Table 3 that ·H generated in the ultrasonic process and Pd^{2+} adsorbed on the surface of NiFe-LDHs reacted to obtain PdNPs. In this process, Pd was coordinated with O in Ni–O and Fe–O, which increased the metal–oxygen bond and promoted PdNPs to anchor more firmly on NiFe-LDHs.

The degradation of 4-NP was used to appraise the performance of Pd/NiFe-LDHs. The results are in Fig. 6.

From Fig. 6, as the reaction progressed, the absorption peak at 400 nm (4-NP) gradually decreased (Mogudi et al. 2016), while the absorption peak at 305 nm (4-AP) gradually increased. With the extension of ultrasonic time, the catalytic performance of the prepared catalysts for 4-NP first increased and then slightly decreased. When the ultrasonic time was 1 h, the time of 4-NP degradation was 5 min. The process of 4-NP degradation followed the Langmuir–Hinshelwood model (Wunder et al. 2010); that is, the negatively charged BH_4^- decomposed into H_2 and BO_2^- on the surface of PdNPs, and each reaction was in line with the pseudo-first-order reaction. The performance of the catalysts was further discussed by calculating the conversion rate (CR), the apparent rate constant (k_a), the normalized ratio constant (k_n), and the turnover rate (TOF), as shown in Table 4. The Pd/NiFe-LDHs prepared with an ultrasonic time of 1 h had the highest TOF value (597.66 h^{-1}), which was much higher than the values of 28.31 h^{-1} for Pd/NiFe-LDHs-C prepared by the chemical method and 35.69 h^{-1} for Pd/C. Table 4 indicates that Pd/NiFe-LDHs prepared by ultrasound have good catalytic performance for 4-NP degradation.

The influence of ultrasonic power

The effect of ultrasonic power (200, 400, 600, 800 W) on the structure, morphology, composition of the catalyst, and performance of the catalytic 4-NP reaction was investigated under the conditions of 1 h, 30 °C, and 5 wt.%.

To understand the effect of ultrasonic power on the structure of the prepared Pd/NiFe-LDHs, an XRD analysis was carried out. The results are in Fig. 7 and Table 5.

It can be seen from Fig. 7 and Table 5 that the value of d(003) decreased as the ultrasonic power increased, which indicated that the layer spacing of NiFe-LDHs became wide without changing the layered structure. Under ultrasonic powers of 600 W and 800 W, the (003) crystal plane diffraction peaks were similar because the increase in the NiFe-LDH layer spacing increased the ultrasonic accommodation degree, and the change in the layer spacing was slight when the power continued to increase.

The effect of ultrasonic power on the morphology of nano Pd on the surface of Pd/NiFe-LDHs was observed by TEM. The results are in Fig. 8.

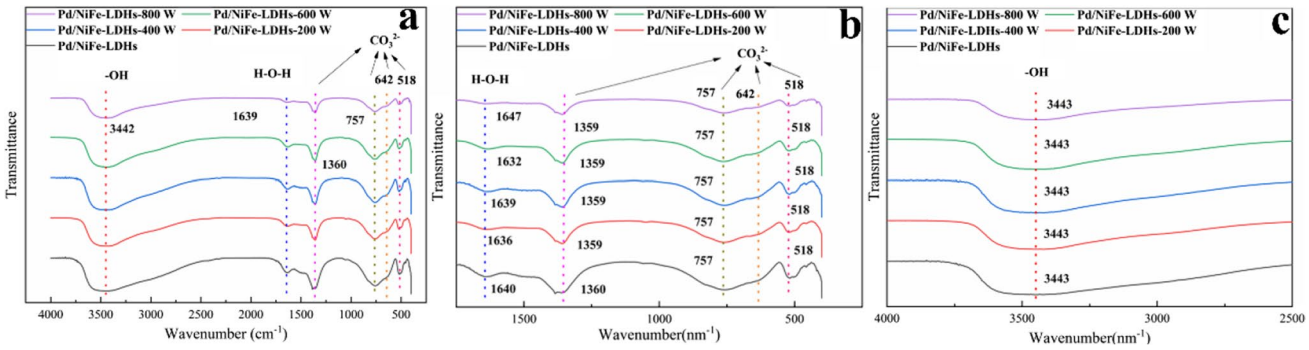

Fig. 10 FT-IR diagrams of Pd/NiFe-LDHs prepared with different ultrasonic power: 4000–425 cm^{-1} (**a**), 1750–425 cm^{-1} (**b**), 4000–2500 cm^{-1} (**c**)

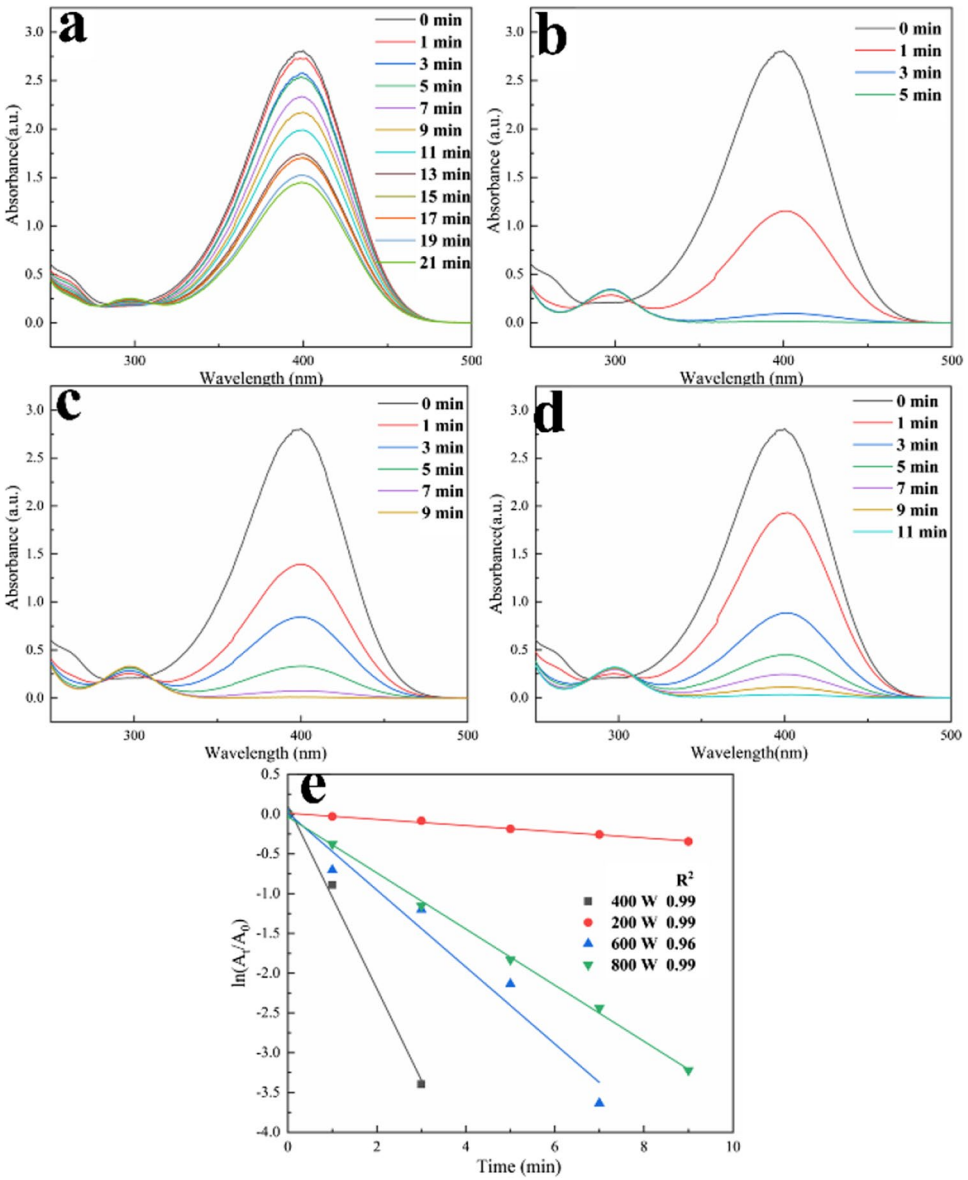

Fig. 11 The effect of ultrasonic power on Pd/NiFe-LDHs catalytic performance of 4-NP degradation: 200 W (**a**), 400 W (**b**), 600 W (**c**), 800 W (**d**), diagram of $\ln(A_t/A_0)$ against reaction time for catalysts prepared at different ultrasonic power (**e**)

From Fig. 8, the reduction degree of Pd^{2+} was very low under an ultrasonic power of 200 W. With increasing ultrasonic power, the concentration of ·H generated by -OH on the surface of NiFe-LDHs increased, and the particle size of PdNPs first increased and then remained unchanged. The average particle size of 1.43 nm at 400 W was the smallest. When ultrasonic power was augmented to 600 W and 800 W continuously, the average particle size increased slightly, which further indicated that the wider layer spacing decreased the effect of ultrasound on NiFe-LDHs. The lattice fringe spacing of the metal in Fig. 9b is 2.29 Å, which corresponds to the Pd(111) crystal plane (Wang and Cao 2007). The above results proved that the surface particles of NiFe-LDHs in the TEM image are PdNPs.

To understand the degree of reduction of Pd caused by ultrasonic power, this study used ultraviolet absorption spectroscopy to detect Pd^{2+} in the supernatant liquid obtained by centrifugation of the catalyst after reduction. The results are in Fig. 9.

There was a Pd^{2+} peak at 445 nm under an ultrasonic power of 200 W in Fig. 9. The absorbance of Pd^{2+} disappeared under an ultrasonic power of 400 W and more, which indicated that Pd^{2+} could not be reduced at 200 W.

FT-IR was used to study the influence of ultrasonic power on the functional groups on the surface of the prepared Pd/NiFe-LDHs. The results are in Fig. 10.

From Fig. 10, the absorption peak at 3443 cm^{-1} was assigned to deformation and the expansion vibration peak of -OH. With increasing ultrasonic power, the intensity of the peaks (518,757 and 3443 cm^{-1}) became slightly weaker, which indicated that the content of CO_3^{2-} and -OH decreased. The migration of the CO_3^{2-} absorption peak

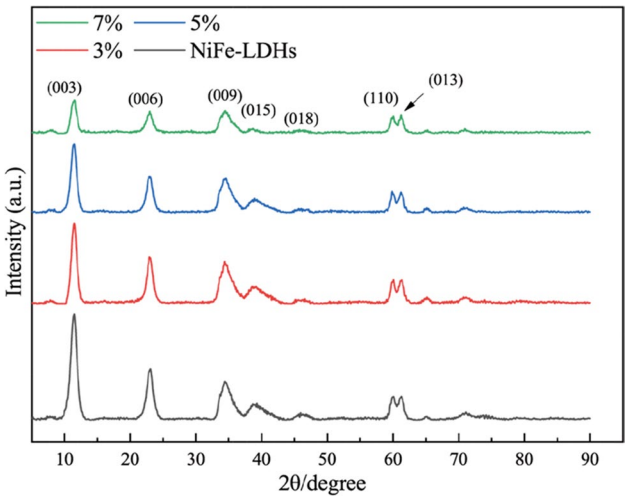

Fig. 12 XRD pattern of Pd/NiFe-LDHs with different Pd loadings

(1360 cm^{-1}) was due to the change in layer spacing by ultrasound, which also led to the reduction of hydrogen bonds between CO_3^{2-} and NiFe-LDHs and made the absorption peak shift toward a lower wavenumber.

Table 6 The lattice parameters of Pd/NiFe-LDHs with different Pd loadings

Samples	d(003)/Å	d(110)/Å	d(113)/Å
NiFe-LDHs	7.77	1.54	1.51
NiFe-LDHs-3.wt %	7.76	1.54	1.51
NiFe-LDHs-5.wt %	7.75	1.54	1.51
NiFe-LDHs-7.wt %	7.71	1.54	1.51

The influence of ultrasonic power on the catalytic 4-NP degradation performance of Pd/NiFe-LDHs was studied. The results are in Fig. 11.

From Fig. 11, the catalytic rate of 4-NP degradation over Pd/NiFe-LDHs first increased and then decreased with increasing ultrasonic power. The catalyst prepared under 400 W had the best catalytic performance.

The influence of Pd loading amount and ultrasonic temperature

The effects of Pd loading (1 wt.%, 3 wt.%, 5 wt.%, 7 wt.%) on the structure and composition of the catalyst and performance of the catalytic 4-NP reaction were investigated under the conditions of 400 W, 30 °C and 1 h.

To study the effect of Pd loading on the structure of the prepared Pd/NiFe-LDH_S, an XRD analysis was carried out. The results are in Fig. 12 and Table 6.

From Fig. 12, d(003) gradually decreased as the Pd loading increased. There were two reasons for this. First, the increase in PdNPs entered the interlayers, and coordination between Pd and O in Fe–O and Ni–O weakened the effect of hydrogen bonding, which enlarged the interlayer spacing of NiFe-LDHs and caused partial peeling of NIFe-LDHs. Therefore, the Pd loading increases and d(003) decreases (Table 6). Second, the successful loading of PdNPs onto NiFe-LDHs concealed part of the NiFe-LDHs.

The influence of Pd loading on the surface functional groups of the prepared Pd/NiFe-LDHs was analyzed by FT-IR. The results are in Fig. 13.

From Fig. 13, an increase in loading has little effect on the surface groups of NiFe-LDHs. In Fig. 14b, the CO_3^{2-} absorption peak at 1360 $cm^{-1}$was slightly shifted and the peak intensity reduced accordingly, it was because the increase in Pd loading rose the interlayer spacing and further increased the contact frequency of CO_3^{2-} with ·H, then more CO_2 was generated, which also led to the reduction of hydrogen bond between CO_3^{2-} and NiFe-LDHs and made the absorption peak shift towards the low wavenumber.

The influence of Pd loading on the catalytic 4-NP degradation performance of Pd/NiFe-LDHs was studied. Results are in Fig. 14.

From Fig. 14, the catalytic rate of 4-NP degradation over Pd/NiFe-LDHs first increased and then decreased with

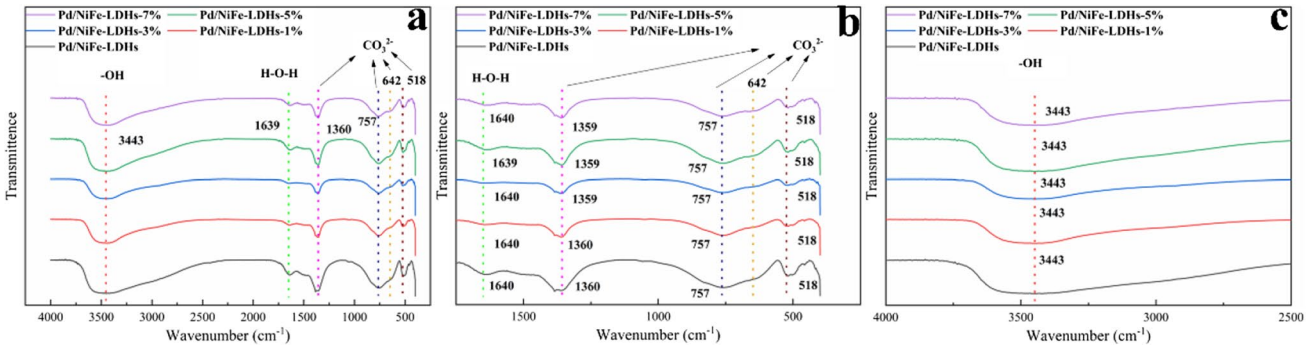

Fig. 13 FT-IR diagrams of Pd/NiFe-LDHs with different Pd loadings: 4000–425 cm^{-1} (**a**), 1750–425 cm^{-1} (**b**), 4000–2500 cm^{-1} (**c**)

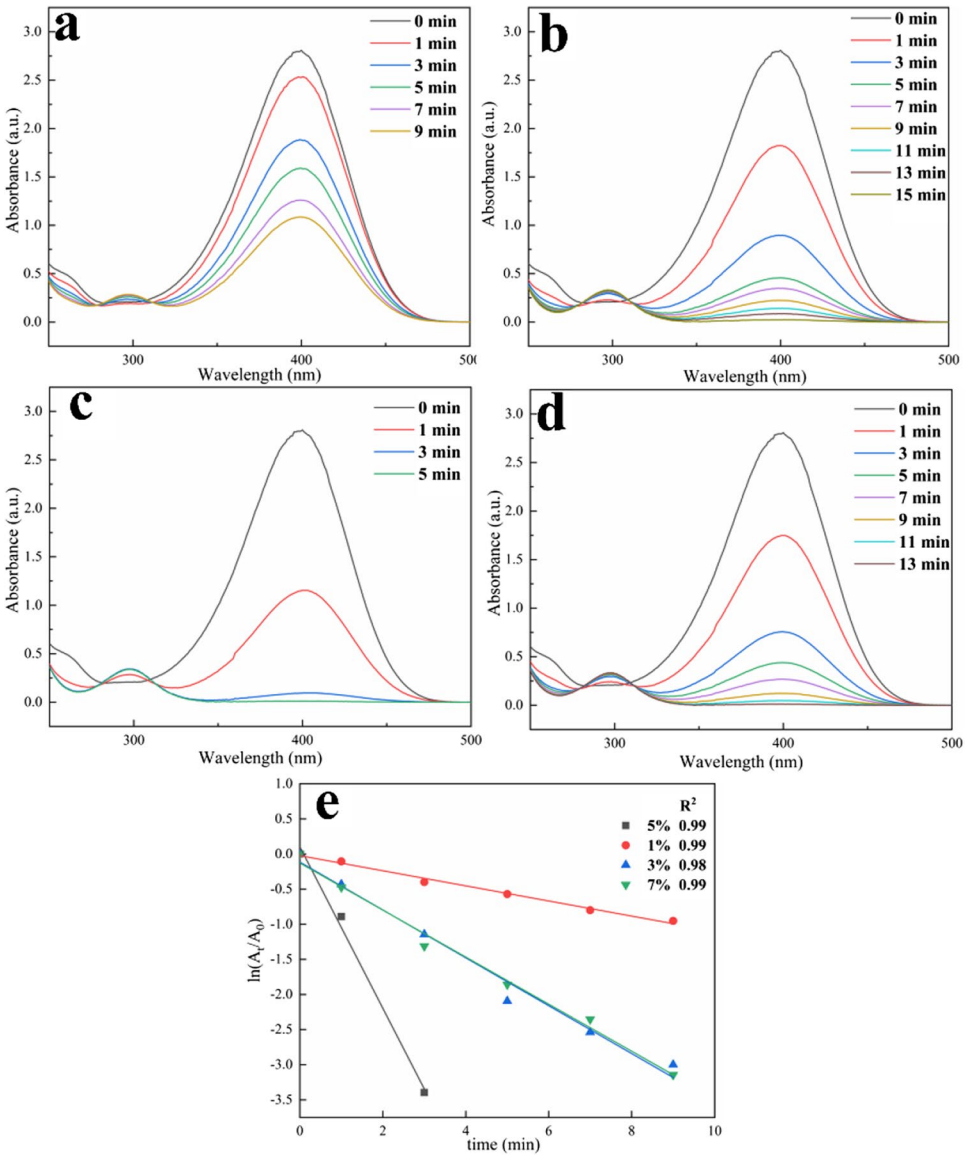

Fig. 14 The effect of Pd loading on Pd/NiFe-LDHs catalytic performance of 4-NP degradation: 1wt.% (**a**), 3wt.% (**b**),5wt.% (**c**), 7wt.% (**d**), diagram of $\ln(A_t/A_0)$ against reaction time for catalysts with different Pd loading (**e**)

increasing Pd loading. It may have better dispersion at low loading, but this will also cause the active components to be separated from each other and reduce the collision frequency of $NaBH_4$ and 4-NP. Therefore, there will be an optimal value for Pd loading. The collision frequency was low when the loading was 1 wt.% and 3 wt.%. The catalyst dispersion was low when the loading was 7 wt.%. Therefore, the catalyst had the best catalytic performance when the loading was 5 wt.%.

The influence of ultrasonic temperature (30 °C, 40 °C, 50 °C, 60 °C) on the catalytic performance of 4-NP degradation was investigated under 400 W for 1 h and a Pd loading of 5 wt.%. The results are in Fig. 15.

Figure 15 shows that the 4-NP degradation rates by catalysts prepared with different ultrasonic temperatures were similar. Therefore, the ultrasonic temperature has little effect on the performance of the prepared catalyst, and the optimum preparation temperature is 30 °C, which has high practical application potential.

The influence of reaction conditions on catalytic performance

The optimal preparation conditions were obtained through the investigation of the preparation conditions. To obtain the optimal reaction conditions for the 4-NP degradation reaction, the effects of $n(NaBH_4)$:n(4-NP), n(Pd):n(4-NP), reaction temperature, and pH were investigated.

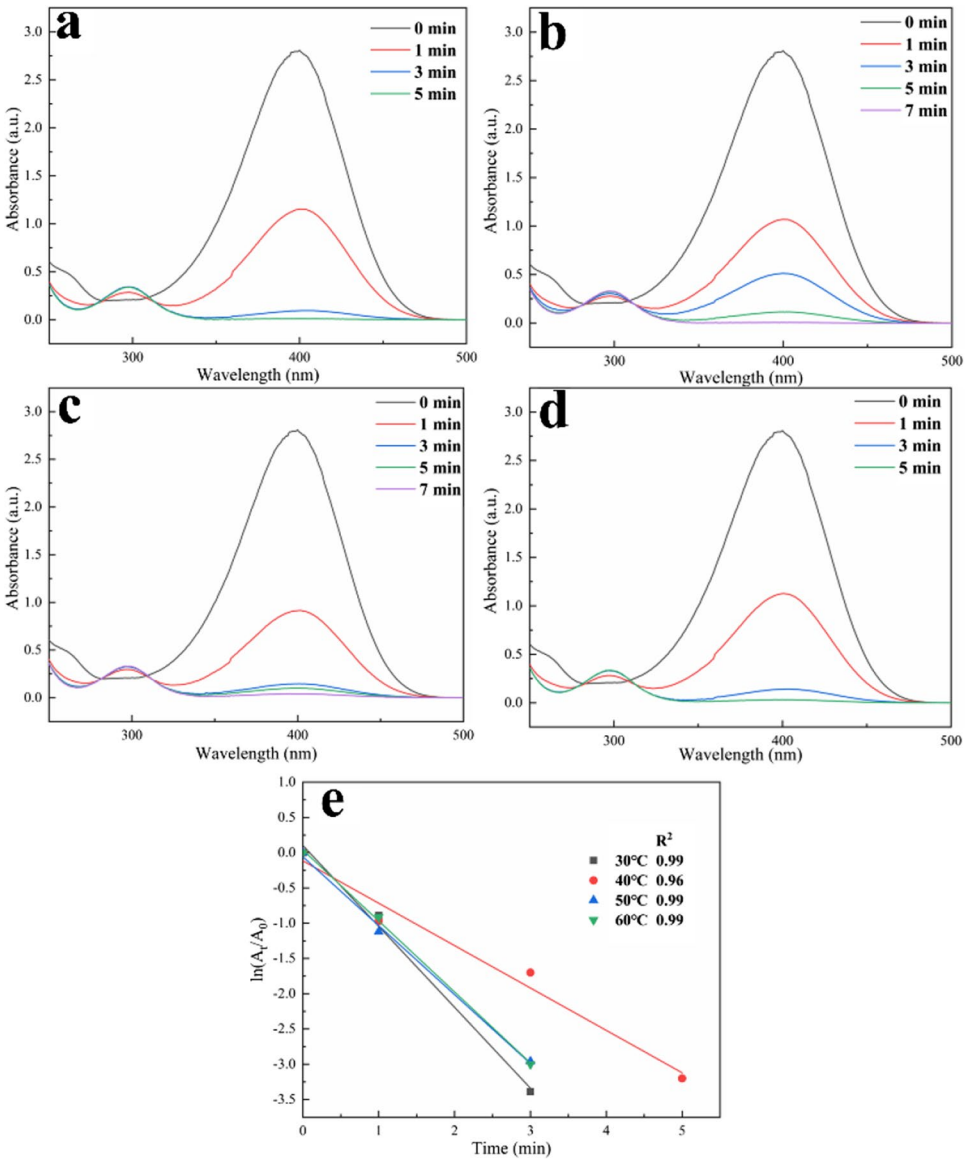

Fig. 15 The effect of ultrasonic temperature on the degradation performance of Pd/NiFe-LDHs catalyzed by 4-NP: 30 °C (**a**), 40 °C (**b**), 50 °C (**c**), 60 °C (**d**), and diagram of $\ln(A_t/A_0)$ against reaction time for catalysts at different ultrasonic temperature (**e**)

The influence of molar ratio of Pd/4-NP

The effect of n(Pd):n(4-NP) on the catalytic performance of 4-NP degradation was studied under n($NaBH_4$):n(4-NP) = 6.67, 30℃, pH = 9.4. Results are in Fig. 16.

From Fig. 16, the degradation rate first increased significantly and then slowly increased as the molar ratio of Pd/4-NP increased. The reason was that the catalysts adsorbed H atoms, BH_4^- and 4-NP to transfer charges to accelerate the reaction, but the adsorption of the catalyst had a certain degree of saturation. When the molar ratio was less than 2%, the catalyst adsorption became supersaturated; therefore, the degradation rate of 4-NP increased significantly with increasing molar ratio. The slow increase in the degradation rate of 4-NP was due to the increase in the active components of catalysts when the molar ratio was 2% and above. Therefore, a 2% molar ratio of catalyst to 4-NP was selected as the optimal dosage of catalyst in this study.

The influence of $NaBH_4$/4-NP molar ratio

The effect of $NaBH_4$/4-NP molar ratio on the catalytic performance of 4-NP degradation reaction was studied under the condition of n(Pd):n(4-NP) = 2%, 30℃, pH = 9.4. Results are in Fig. 17.

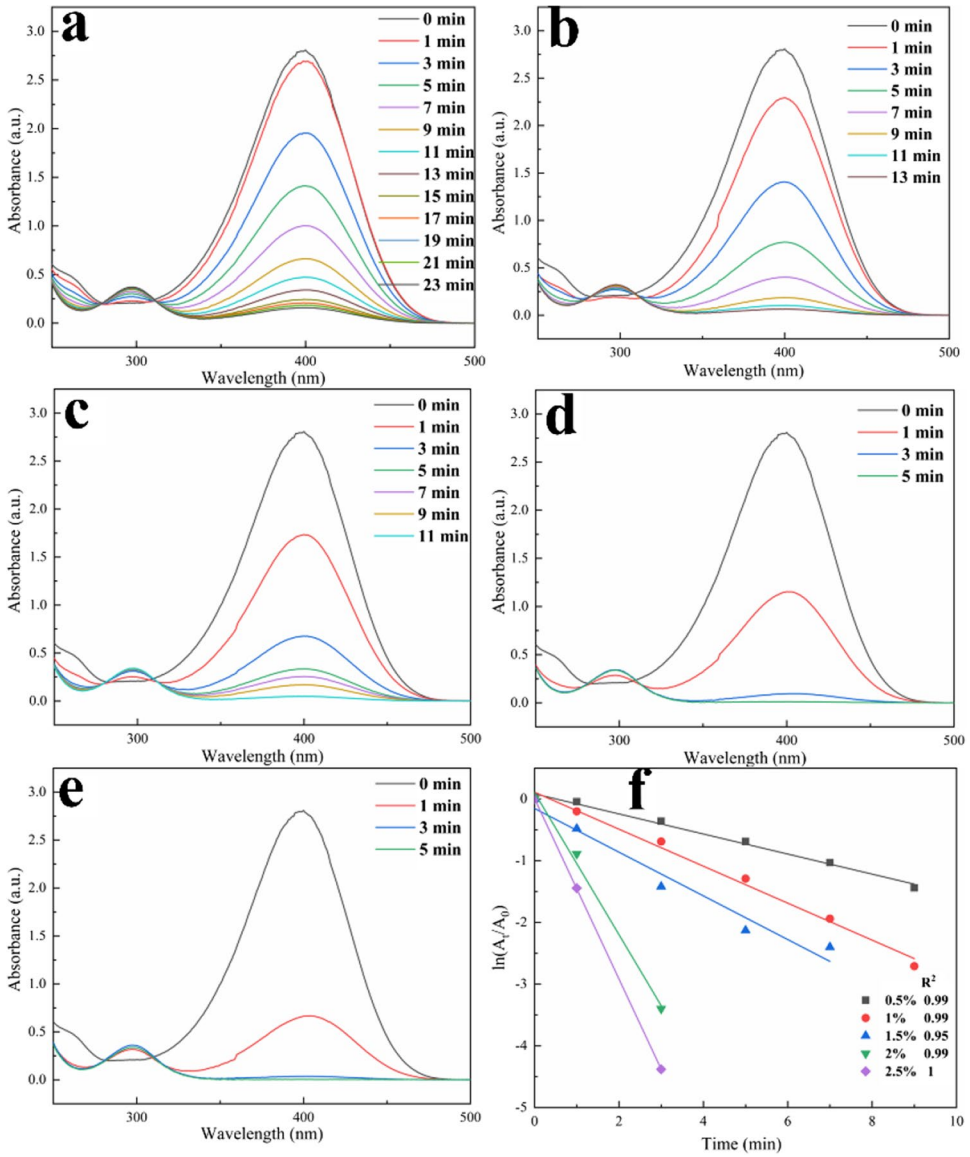

Fig. 16 The affection of n(Pd):n(4-NP) on degradation reaction of 4-NP: 0.5% (**a**), 1% (**b**), 1.5% (**c**), 2% (**d**), 2.5% (**e**), and diagram of $\ln(A_t/A_0)$ against reaction time for catalysts with different molar ratio of Pd/4-NP (**f**)

From Fig. 17, the degradation rate first increased significantly and then slowly increased as the molar ratio of $NaBH_4$/4-NP rose. This was the pseudo-first-order reaction when n($NaBH_4$):n(4-NP) was 6, so the reaction rate in the early stage was faster with increasing time when n($NaBH_4$):n(4-NP) was 5 times or less. The amount of M-H produced was insufficient in the later stage, which was not a pseudo-first-order reaction and would cause a decrease in the catalytic reaction rate. The whole reaction process was a pseudo-first-order reaction. When n($NaBH_4$):n(4-NP) was 6.7, the reaction rate became fast, and the amount of $NaBH_4$ continued to increase; the reaction rate increased slightly. Therefore, the optimal n($NaBH_4$):n(4-NP) was 6.7.

The influence of reaction temperature

The affection of reaction temperature on catalytic performance of 4-NP degradation was studied under the conditions of n(Pd):n(4-NP) = 2%, n($NaBH_4$):n(4-NP) = 6.67, pH = 9.4. In the 20 mL reaction system, $NaBH_4$, 4-NP and catalyst were the same proportions as the cuvette reaction system and reacted at 20℃, 30℃, 40℃, and 50℃, taking 2 mL each time, and then detected in a cuvette. The results are shown in Fig. 18.

From Fig. 18, the 4-NP degradation rate first increased and then decreased as the reaction temperature increased. The 4-NP degradation rate was the fastest at 30 °C. As the temperature increased further, the particles became

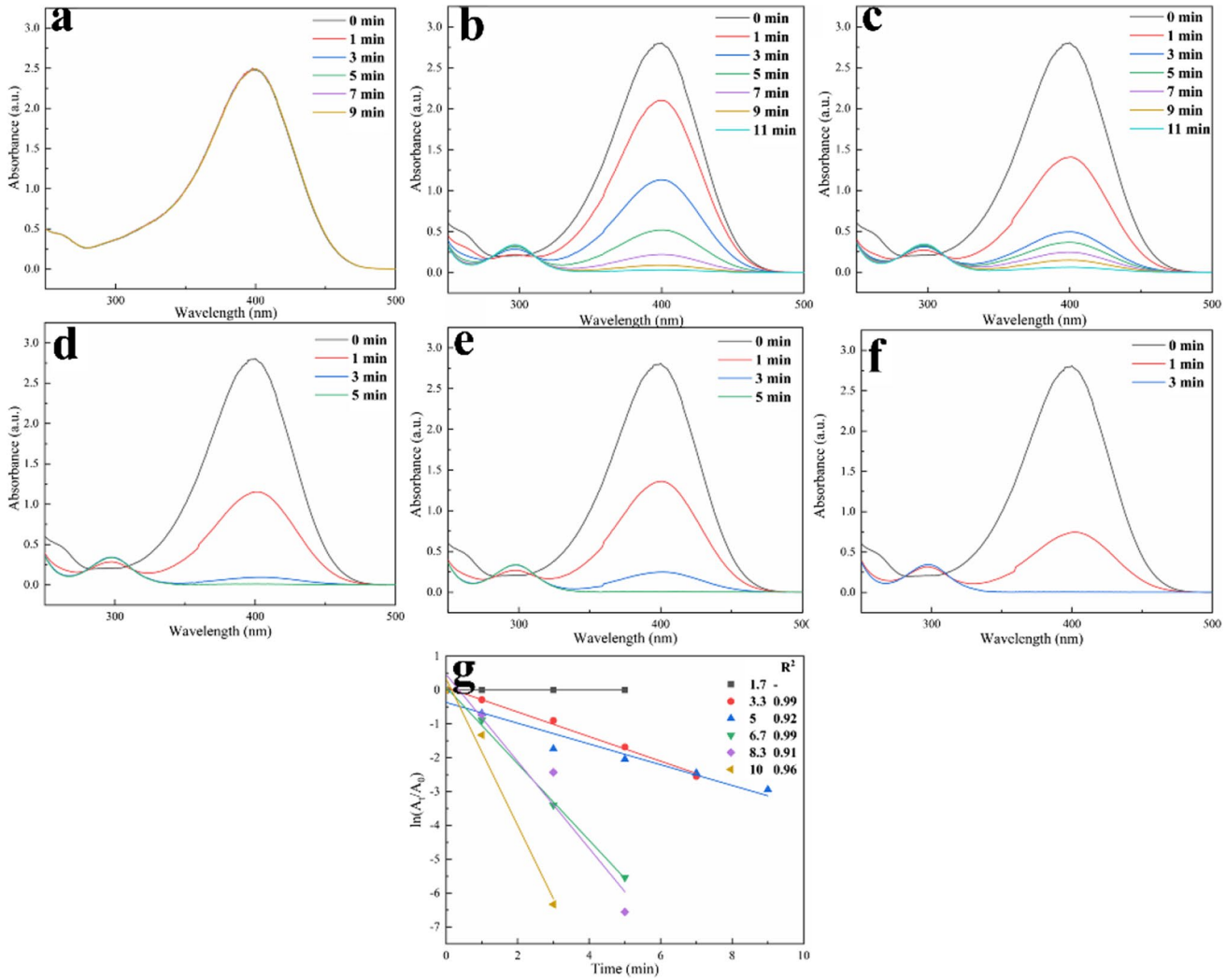

Fig. 17 The influence of n($NaBH_4$):n(4-NP) on the degradation reaction of 4-NP: 1.7 (**a**), 3.3 (b), 5 (**c**), 6.7 (**d**), 8.3 (**e**), 10 (**f**), diagram of ln(A_t/A_0) against reaction time for catalysts with different $NaBH_4$/4-NP molar ratio (**g**)

more active, but the ability of the catalyst to adsorb $NaBH_4$ and 4-NP decreased, so the reaction rate decreased slowly. Therefore, the reaction rate was the fastest at 30 °C, which was more in line with actual application conditions and had actual production potential.

The influence of pH

The pH of the 4-NP degradation reaction system will affect the reaction rate. First, reactants (BH_4^- and 4-NP) are adsorbed on the surface of the catalyst, and BH_4^- is catalyzed by the catalyst to decompose into H radicals and BH_3^-. The increase in the concentration of H^+ rose the amount of H^+ adsorbed by the catalyst, while the polarity of NO_2^- in 4-NP decreased due to an increase in the amount of H^+, which led to the difficulty of being absorbed by the catalyst. Therefore, the catalytic efficiency decreased. At the same time, the unabsorbed BH_4^- reacted with H^+ quickly to generate H_2 and left from the reaction system, which would reduce the amount of BH_4^- and the rate of 4-NP reduction significantly. A high pH would inhibit the decomposition of $NaBH_4$ into H_2, and reduce the reducibility to reduce the catalytic rate. Therefore, it was necessary to investigate pH of the reaction system. The affection of pH on catalytic performance of 4-NP degradation reaction was investigated under the condition of n(Pd):n(4-NP) = 2%, n($NaBH_4$):n(4-NP) = 6.67,30℃. The pH was changed by adding a small amount of NaOH and HCl. Results are in Fig. 19.

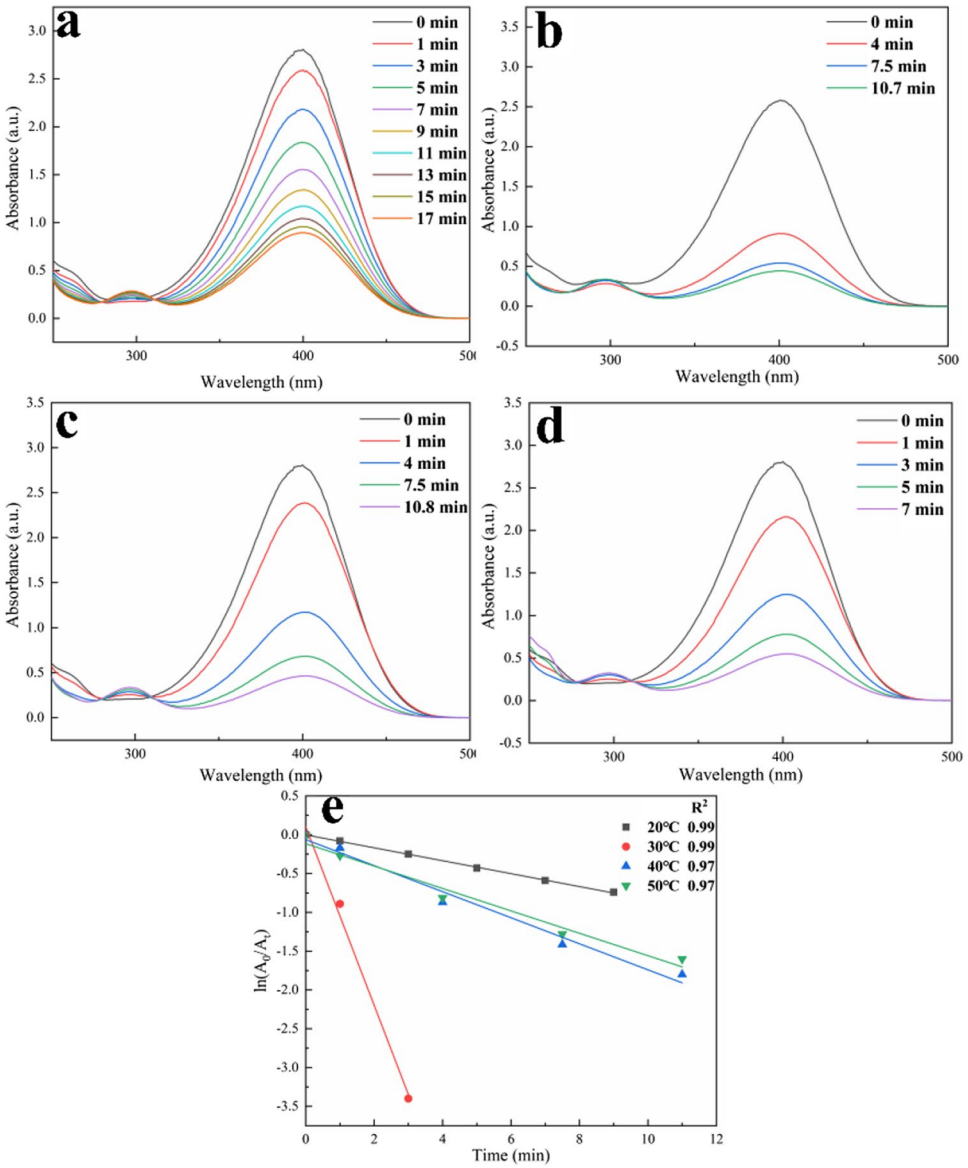

Fig. 18 The influence of reaction temperature on 4-NPdegradation: 20 °C (**a**), 30 °C (**b**), 40 °C (**c**), 50 °C (**d**), (e) diagram of $\ln(A_t/A_0)$ against reaction time for catalysts with different reaction temperature

From Fig. 19, the 4-NPdegradationratefirst increased and then decreased as the pH increased. The reaction rate was the highest when the pH was 9.5, which was the best condition.

Investigation of catalyst stability

A 500 mL reaction system was used in this study to investigate the stability of Pd/NiFe-LDHs. The system changed from light yellow to colorless after 10 min under the conditions of $n(NaBH_4):n(4\text{-NP}) = 6.67$, $n(Pd):n(4\text{-NP}) = 2\%$,30℃. Two milligrams of the reaction solution was used to detect the conversion rate of 4-NP. The same amount of $NaBH_4$ and 4-NP was added for the first time to the reaction system after the first reaction, and it became colorless after 10 min. Then, the conversion rate of 4-NP was checked again, and the cycle reaction was repeated 10 times. From Fig. 20, the conversion rate of the 10th reaction was still as high as 98.75%, which indicated that the catalyst has good stability.

Investigation of catalyst adaptability

In this study, the reduction reaction of three toxic dyes, congo red (CR), methylene blue (MB), and methyl orange (MO) was used to test the suitability of the catalyst. Three dye solutions of 1 mg/mL and $NaBH_4$ solution of 0.02 M were prepared respectively. 0.8 mL of dye solution and 1.6 mL of $NaBH_4$ solution were put into a colorimetric dish.

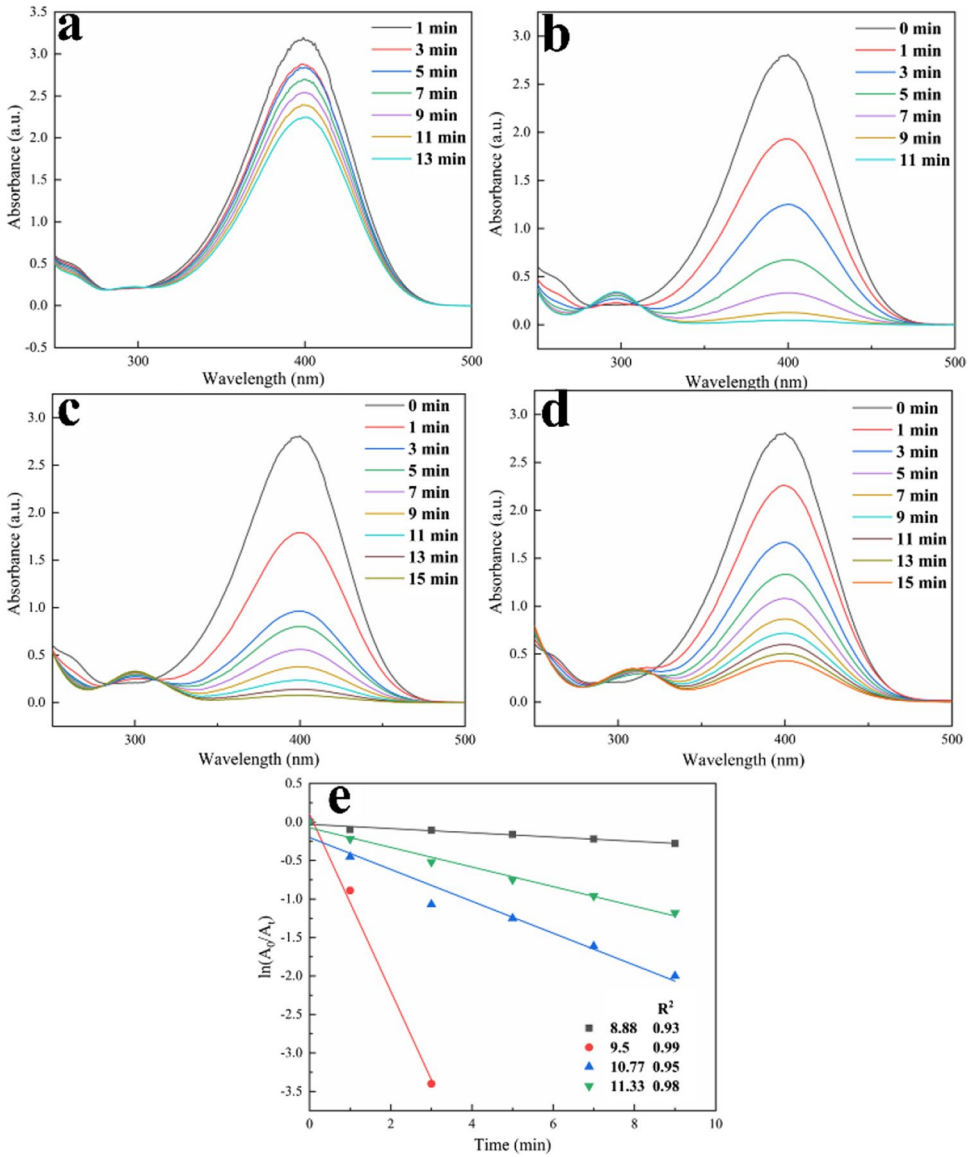

Fig. 19 The effect of pH on 4-NPdegradation: 8.88 (**a**), 9.50 (**b**), 10.77 (**c**), 11.33 (**d**), diagram of $\ln(A_t/A_0)$ against reaction time for catalysts at different pH (**e**)

Then some deionized water was added to make the final reaction system 4 mL, and the catalyst containing 1.2 μmol, and 1.2 μmol, 0.6 μmol, and 0.18 μmol of Pd was added to the CR, MO, and MB solutions, respectively. Results are in Fig. 21.

In this study, the change of dye concentration in solution with time was detected by the intensity change of the ultraviolet characteristic absorption peak of several dyes. Among them, the peak at 493 nm (Fig. 21a) was ascribed to CR, and the peaks at 465 nm (Fig. 21b) and 664 nm (Fig. 21c) were ascribed to MO and MB, respectively (Rahmani et al. 2014). The reaction of the three solutions was completed within 10 min under the reduction of the same concentration of $NaBH_4$. A very small amount of catalysts could efficiently and quickly catalyze these reduction processes at room temperature, which indicated that the catalyst is also suitable for the degradation of other pollutants and has high practical application potential.

Preparation and degradation mechanism

Pd^{2+} reducing mechanism

Blank experiments were investigated on the preparation of $Pd/NiFe\text{-}LDH_S$. Results are in Fig. 22.

From Fig. 22a, the absorption peak intensity of Pd^{2+} under ultrasound did not change significantly in the Pd^{2+}-H_2O system, which indicated that H_2O could not reduce Pd^{2+} under the action of ultrasound.

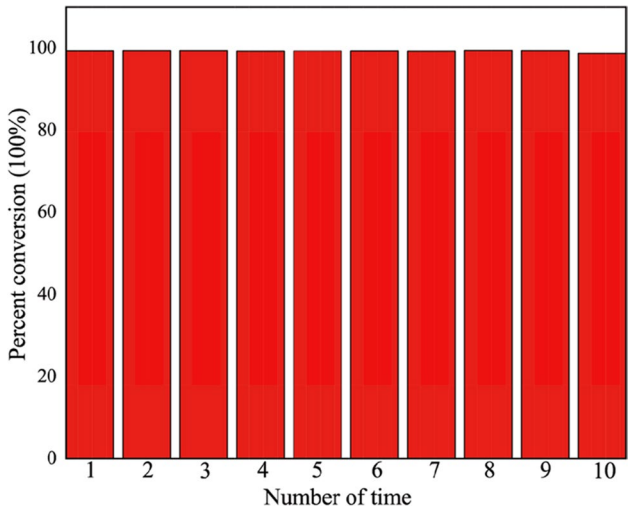

Fig. 20 Reusability of Pd/NiFe-LDHs

NiFe-LDH-H_2O system, which indicated that the surface hydroxyl group of NiFe-LDHs had difficulty reducing Pd^{2+} without ultrasound. From Fig. 22c, the intensity of the Pd^{2+} absorption peak (415 nm) gradually decreased over time and disappeared at 30 min completely under the action of ultrasound in the Pd^{2+}/NiFe-LDH-H_2O system. Pd^{2+} can be quickly reduced only when NiFe-LDHs and ultrasound are present at the same time.

From the above analysis, the hydroxyl on the surface of NiFe-LDHs can be dissociated to highly reductive H radicals and react with the Pd^{2+} adsorbed on the surface of NiFe-LDHs under the action of ultrasound. Pd^{2+} can be reduced to Pd^0 by ultrasonic treatment at 30℃ for a certain time without reducing agents and stabilizing agents. The reactions involved are in Fig. 23.

As shown in Fig. 23, the formation of stable PdNPs in NiFe-LDHs under the action of ultrasound can be put down to the following points: (1) NiFe-LDHs could

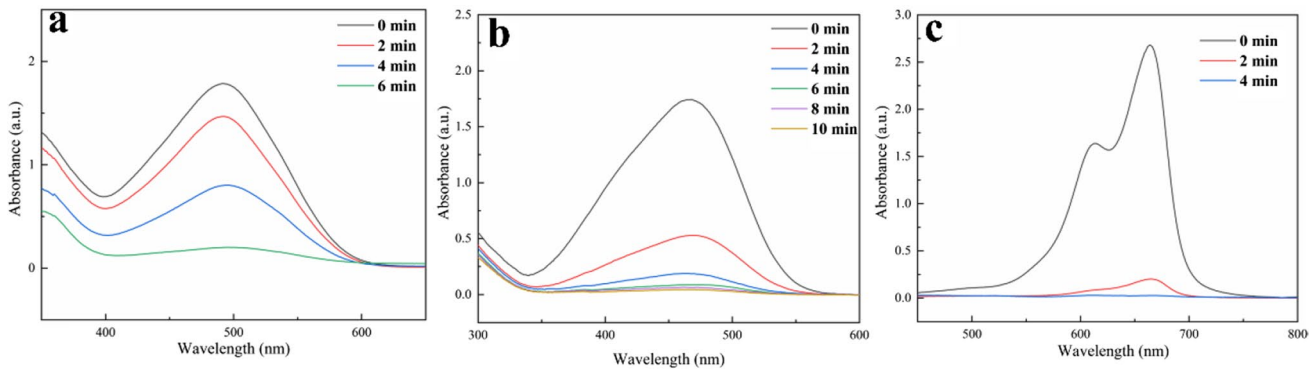

Fig. 21 UV–Vis spectra of CR, MB and MO in MB, CR and MO degradation over time: CR (**a**), MO (**b**), MB (**c**)

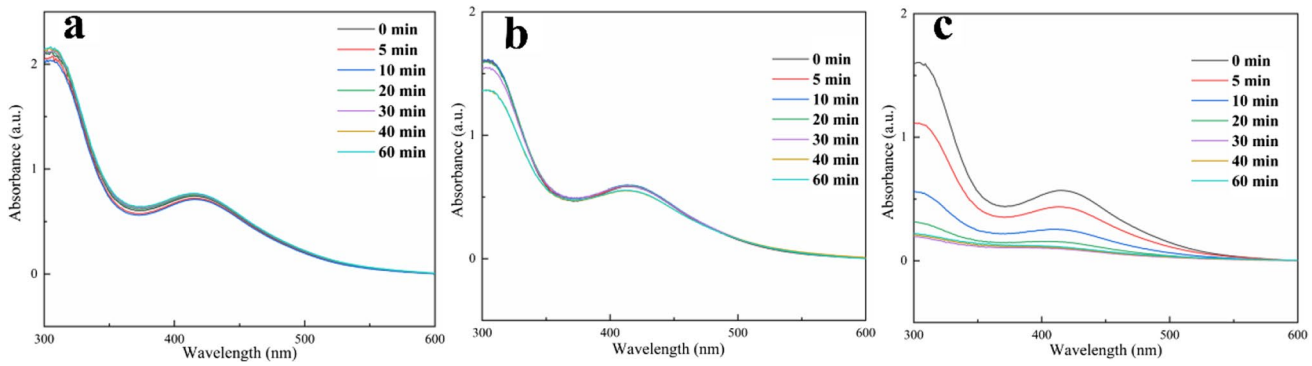

Fig. 22 UV–Vis spectra of Pd^{2+}-H_2O with ultrasound (**a**), Pd^{2+}/NiFe-LDH-H_2O without ultrasound (**b**), Pd^{2+}/NiFe-LDHs-OH with ultrasound at different times (**c**)

Figure 22b shows that absorption peak intensity of Pd^{2+} had no obvious change without ultrasound in the Pd^{2+}/ adsorb Pd^{2+}, and the dissociated H from hydroxyl on the surface of it could reduce Pd^{2+} to Pd^0 with the action of

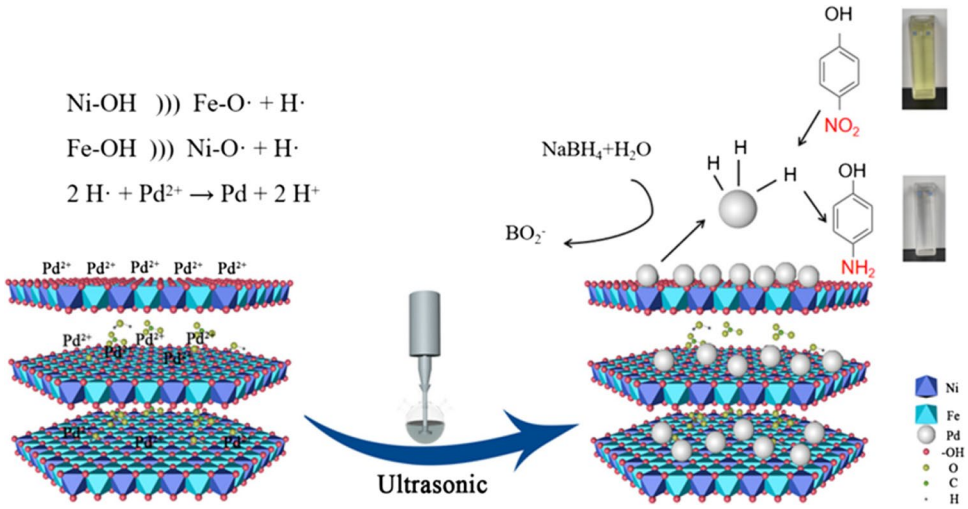

Fig. 23 Mechanism of preparation of Pd/NiFe-LDHs nanocatalyst and Mechanism of degradation of 4-NP

Table 7 Catalytic performance of Pd/NiFe-LDHs

Catalyst	k_a (min)	K_n ($mg^{-1}·min^{-1}$)	TOF (h^{-1})	Reference
Pd/NiFe-LDHs	1.147	47.79	597.66	This work
Pd/SPB-PS	0.0264	0.116	nd	Mei (2007)
Np-Ag–Al	2.16	nd	114.6	Li et al. (2015)
Au/g-C3N4-6	7.9895	nd	115.7	Fu et al. (2017)
HA-Pd NPs	0.643	nd	131.07	Yin et al. (2020)
Au NPs	nd	nd	74.16	Lin et al. (2013)

nd not detected.

ultrasound. (2) Pd/NiFe-LDHs had good stability because Pd^{2+} on the surface of NiFe-LDHs was reduced in situ during the ultrasonic process and the reduced PdNPs anchored to the surface of NiFe-LDHs. (3) The surface of NiFe-LDHs was rich in hydroxyl groups that could coordinate with PdNPs, which was beneficial for anchoring PdNPs.

Degradation mechanism

The pseudo-first-order reaction between 4-NP and $NaBH_4$ is as follows.

It can be seen from the equations that BH_4^- can be dissociated to M-BH_3^- and M-H by M(Pd), and the 4-NP can be reduced to 4-AP by M-H. The degradation reaction of 4-NP can be regarded as a pseudo-first-order reaction when BH_4^- is 6 times that of 4-NP.

From Table 7, Pd/NiFe-LDHs had a higher TOF value than other literature, which indicated that Pd/NiFe-LDHs had a desirable catalytic performance for 4-NP degradation.

Conclusion

NiFe-layered double hydroxides (NiFe-LDHs) loaded ultrafine nano Pd catalysts (Pd/NiFe-LDHs) were prepared by a facile ultrasonic-assisted in situ reduction technology without any stabilizing agents and reducing agents. During this process, reduction of Pd^{2+} and loading of PdNPs occurred simultaneously. The ultrasonic preparation process caused the XPS characteristic peaks of Fe 2p and Ni 2p to shift to the direction of low binding energy and caused the characteristic peaks of Pd 3d shift to high binding energy, which proved that PdNPs coordinated with O in Ni–O and Fe–O during the reaction and improved the stability of the catalyst. At the same time, the decrease of the d(003) in XRD indicated that Pd^{2+} had entered the interlayer, and Pd^{2+} was reduced to PdNPs by the ·H produced by the interlayer -OH. Then PdNPs stayed in the interlayer, which enlarged the interlayer spacing and caused partial peeling of NiFe-LDHs. TEM results showed that this preparation method had obtained PdNPs with a particle size of 1.43 nm. In the activity test, the catalyst could completely degrade 4-NP within 5 min, with a TOF value of 597.66 $h^{-1}$was 16.7 times that of commercial Pd/C. In the stability test, the 4-NP conversion rate remained 98.75% after ten cycles. In addition, the catalyst also has desirable catalytic activity for CR, MB, and MO degradation. Therefore, the ultrasound-assisted preparation of ultrafine metal nanoparticles is a green and efficient method, and it has significant application potential in the synthesis of ultrafine metal nanoparticles.

Acknowledgements This work was supported by the National Key R&D Program (2018YFE0108800), the National Natural Science Foundation of China (21676074), and the Science Foundation of Heilongjiang Academy of Sciences (KY2020SH01&WS2021SH01).

Author contribution All authors contributed to the study conception and design. Material preparation and data collection and analysis were performed by Xuan Zhou, Jiaming Shi, and Xuefeng Bai. The first draft of the manuscript was written by Xuan Zhou and all authors commented on previous versions of the manuscript. All authors read and approved the final manuscript.

Conceptualization: Xuefeng Bai and Xuan Zhou; Methodology: Xuan Zhou; Formal analysis and investigation: Xuan Zhou; Writing—original draft preparation: Xuan Zhou; writing—review and editing: Xuefeng Bai; Funding acquisition: Xuefeng Bai; Resources: Xuefeng Bai; Supervision: Xuefeng Bai and Jiaming Shi.

Funding This work was supported by the National Key R&D Program (2018YFE0108800), the National Natural Science Foundation of China (21676074), and the Science Foundation of Heilongjiang Academy of Sciences (KY2020SH01 and WS2021SH01).

Data availability The datasets used and analyzed during the current study are available from the corresponding author on reasonable request.

Declarations

Ethics approval and consent to participate Not applicable.

Consent for publication Not applicable.

Competing interests The authors declare no competing interests.

References

Abdelhamid HN (2021) High performance and ultrafast reduction of 4-nitrophenol using metal-organic frameworks. J Environ Chem Eng 9(1):104404. https://doi.org/10.1016/j.jece.2020.104404

Abellán G, Carrasco JA, Coronado E et al (2014) In-situ growth of ultrathin films of NiFe-LDHs: towards a hierarchical synthesis of bamboo-like carbon nanotubes. Adv Mater Interfaces 1(6):1400184. https://doi.org/10.1002/admi.201400184

Al-Kahtani AA, Almuqati T, Alhokbany N et al (2018) A clean approach for the reduction of hazardous 4-nitrophenol using gold nanoparticles decorated multiwalled carbon nanotubes. J Clean Prod 191:429–435. https://doi.org/10.1016/j.jclepro.2018.04.197

Allman A, Daoutidis P, Arnold WA et al (2019) Efficient water pollution abatement. Ind Eng Chem Res 58(50):22483–22487. https://doi.org/10.1021/acs.iecr.9b03241

Anantharaj S, Karthick K, Venkatesh M et al (2017) Enhancing electrocatalytic total water splitting at few layer Pt-NiFe layered double hydroxide interfaces. Nano Energy 39:30–43. https://doi.org/10.1016/j.nanoen.2017.06.027

Bashir MS, Jiang X, Kong XZ (2020) Porous polyurea microspheres with Pd immobilized on surface and their catalytic activity in 4-nitrophenol reduction and organic dyes degradation. Eur Polymer J 129:109652. https://doi.org/10.1016/j.eurpolymj.2020.109652

Bogireddy NKR, Sahare P, Pal U et al (2020) Platinum nanoparticle-assembled porous biogenic silica 3D hybrid structures with outstanding 4-nitrophenol degradation performance. Chem Eng J 388:124237. https://doi.org/10.1016/j.cej.2020.124237

Bose B (2010) Global warming: energy, environmental pollution and the impact of power electronics. IEEE Ind Electron Mag 4:6–17. https://doi.org/10.1109/MIE.2010.935860

Cai Y, Yang F, Wu L et al (2021) Hydrothermal-ultrasonic synthesis of CuO nanorods and $CuWO_4$ nanoparticles for catalytic reduction, photocatalysis activity, and antibacterial properties. Mater Chem Phys 258:123919. https://doi.org/10.1016/j.matchemphys.2020.123919

Chu C, Rao S, Ma Z et al (2019) Copper and cobalt nanoparticles doped nitrogen-containing carbon frameworks derived from CuO-encapsulated ZIF-67 as high-efficiency catalyst for hydrogenation of 4-nitrophenol. Appl Catal B 256:117792. https://doi.org/10.1016/j.apcatb.2019.117792

Cipagauta-Diaz S, Estrella-González A, Gomez R (2019) Heterojunction formation on $InVO_4$/N-TiO_2 with enhanced visible light photocatalytic activity for reduction of 4-NP. Mater Sci Semicond Process 89:201–211. https://doi.org/10.1016/j.mssp.2018.09.017

Dai H, Deng Z, Zeng Y et al (2020) Highly sensitive determination of 4-nitrophenol with coumarin-based fluorescent molecularly imprinted poly (ionic liquid). J Hazard Mater 398:122854. https://doi.org/10.1016/j.jhazmat.2020.122854

Dunn K, Yen TF (2001) A plausible reaction pathway of asphaltene under ultrasound. Fuel Process Technol 73(1):59–71. https://doi.org/10.1016/S0378-3820(01)00194-1

Fang B, Xing Z, Sun D, et al (2021) Hollow semiconductor photocatalysts for solar energy conversion. Adv Powder Mater 1(2):100021. https://doi.org/10.1016/j.apmate.2021.11.008

Fu Y, Huang T, Jia B, Zhu J, Wang X (2017) Reduction of nitrophenols to aminophenols under concerted catalysis by Au/g-C3N4 contact system. Appl Catal B Environ 202:430–437. https://doi.org/10.1016/j.apcatb.2016.09.051

Ge S, Gu J, Ai W et al (2021) Biotreatment of pyrene and Cr (VI) combined water pollution by mixed bacteria. Sci Rep 11(1):1–7. https://doi.org/10.1038/s41598-020-80053-2

Gu Y, Wang Y, An W et al (2019) A novel strategy to boost the oxygen evolution reaction activity of NiFe-LDHs with in situ synthesized 3D porous reduced graphene oxide matrix as both the substrate and electronic carrier. New J Chem 43(17):6555–6562. https://doi.org/10.1039/C9NJ00518H

Gültekin I, Ince NH (2006) Degradation of aryl-azo-naphthol dyes by ultrasound, ozone and their combination: effect of α-substituents. Ultrason Sonochem 13(3):208–214. https://doi.org/10.1016/j.ultsonch.2005.03.002

Gupta VK, Atar N, Yola ML et al (2014) A novel magnetic Fe@ Au core–shell nanoparticles anchored graphene oxide recyclable nanocatalyst for the reduction of nitrophenol compounds. Water Res 48:210–217. https://doi.org/10.1016/j.watres.2013.09.027

Gursky JA, Blough SD, Luna C et al (2006) Particle− particle interactions between layered double hydroxide nanoparticles. J Am Chem Soc 128(26):8376–8377. https://doi.org/10.1021/ja0612100

Hou CY, Wang C, Xing YH et al (2020) Fluorescence detection of metals and nitro aromatic compounds based on tetrastyrene derivatives. J Inorg Organomet Polym Mater 30(4):1162–1171. https://doi.org/10.1007/s10904-019-01283-0

Hu H, Wageh S, Al-Ghamdi AA et al (2020) NiFe-LDH nanosheet/carbon fiber nanocomposite with enhanced anionic dye adsorption performance. Appl Surf Sci 511:145570. https://doi.org/10.1016/j.apsusc.2020.145570

Jaleh B, Karami S, Sajjadi M et al (2020) Laser-assisted preparation of Pd nanoparticles on carbon cloth for the degradation of environmental pollutants in aqueous medium. Chemosphere 246:125755. https://doi.org/10.1016/j.chemosphere.2019.125755

Kose M, Kırpık H, Kose A et al (2019) New Sm (III) and Nd (III) complexes: Synthesis, structural characterization and fluorescent sensing of nitro-aromatic compounds. Appl Organomet Chem 33(5):e4843. https://doi.org/10.1002/aoc.4843

Kubendhiran S, Sakthivel R, Chen SM et al (2018) Innovative strategy based on a novel carbon-black− β-cyclodextrin nanocomposite for the simultaneous determination of the anticancer drug flutamide and the environmental pollutant 4-nitrophenol. Anal Chem 90(10):6283–6291. https://doi.org/10.1021/acs.analchem.8b00989

Ledendecker M, Krick Calderón S, Papp C et al (2015) The synthesis of nanostructured Ni_5P_4 films and their use as a non-noble bifunctional electrocatalyst for full water splitting. AngewandteChemie Int Ed 54(42):12361–12365. https://doi.org/10.1002/anie.201502438

Li J, Liu C, Liu Y (2012) Au/graphene hydrogel: synthesis, characterization and its use for catalytic reduction of 4-nitrophenol. J Mater Chem 22(17):8426–8430. https://doi.org/10.1039/c2jm16386a

Li Z et al (2015) Facile reduction of aromatic nitro compounds to aromatic amines catalysed by support-free nanoporous silver. RSC Adv 5(38):30062–30066. https://doi.org/10.1039/c5ra01649e

Li H, Zhu X, Tang Q et al (2020) Three-dimensional NiFe layered double hydroxide nanowire/nanoporous ni/nickel foam for efficient oxygen evolution. J Electrochem Soc 167(14):146513. https://doi.org/10.1149/1945-7111/abc7e7

Li J, Bai X, Lv H (2020) Ultrasonic-assisted reduction for facile synthesis of ultrafine supported Pd nanocatalysts by hydroxyl groups on the surfaces of layered double hydroxides and their catalytic properties. Ultrason Sonochem 60:104746. https://doi.org/10.1016/j.ultsonch.2019.104746

Liang J, Shen H, Ma Y et al (2020) Autogenous growth of the hierarchical V-doped NiFe layer double metal hydroxide electrodes for an enhanced overall water splitting. Dalton Trans 49(32):11217–11225. https://doi.org/10.1039/D0DT01520B

Lin C, Tao K, Hua D et al (2013) Size effect of gold nanoparticles in catalytic reduction of p-nitrophenol with $NaBH_4$. Molecules 18(10):12609–12620. https://doi.org/10.3390/molecules181012609

Liu Y, Yang Z (2016) Intercalation of sulfate anions into a Zn–Al layered double hydroxide: their synthesis and application in Zn–Ni secondary batteries. RSC Adv 6(73):68584–68591. https://doi.org/10.1039/C6RA09096F

Liu P, Zhao M (2009) Silver nanoparticle supported on halloysite nanotubes catalyzed reduction of 4-nitrophenol (4-NP). Appl Surf Sci 255(7):3989–3993. https://doi.org/10.1016/j.apsusc.2008.10.094

Liu QS, Zheng T, Wang P et al (2010) Adsorption isotherm, kinetic and mechanism studies of some substituted phenols on activated carbon fibers. Chem Eng J 157(2–3):348–356. https://doi.org/10.1016/j.cej.2009.11.013

Liu S, Wang J, Huang W et al (2019) Adsorption of phenolic compounds from water by a novel ethylenediamine rosin-based resin: interaction models and adsorption mechanisms. Chemosphere 214:821–829. https://doi.org/10.1016/j.chemosphere.2018.09.141

Liu M, Yang H, Xu Z et al (2020) The green synthesis of PdO/Pd anchored on hierarchical ZnOmicroflowers with a synthetic effect for the efficient catalytic reduction of 4-nitrophenol. New J Chem 44(17):7035–7041. https://doi.org/10.1039/D0NJ00001A

Liu T, Sun Y, Jiang B et al (2020b) Pd Nanoparticle-decorated 3D-printed hierarchically porous TiO_2 scaffolds for the efficient reduction of a highly concentrated 4-nitrophenol solution. ACS Appl Mater Interfaces 12(25):28100–28109. https://doi.org/10.1021/acsami.0c03959

Lu Y, Jiang B, Fang L et al (2016) High performance NiFe layered double hydroxide for methyl orange dye and Cr (VI) adsorption. Chemosphere 152:415–422. https://doi.org/10.1016/j.chemosphere.2016.03.015

Mahalakshmi G, Rajeswari M, Ponnarasi P (2020) Synthesis of few-layer g-C3N4 nanosheets-coated MoS_2/TiO_2 heterojunction photocatalysts for photo-degradation of methyl orange (MO) and 4-nitrophenol (4-NP) pollutants. Inorg Chem Commun 120:108146. https://doi.org/10.1016/j.inoche.2020.108146

Mei Y (2007) Catalytic activity of palladium nanoparticles encapsulated inspherical polyelectrolyte brushes and core-shell microgels. Chem Mater 19(5):1062–1069. https://doi.org/10.1021/cm062554s

Mogudi BM, Ncube P, Meijboom R (2016) Catalytic activity of mesoporous cobalt oxides with controlled porosity and crystallite sizes: evaluation using the reduction of 4-nitrophenol. Appl Catal B 198:74–82. https://doi.org/10.1016/j.apcatb.2016.05.051

Mohammadi Z, Entezari MH (2018) Sono-synthesis approach in uniform loading of ultrafine Ag nanoparticles on reduced graphene oxide nanosheets: an efficient catalyst for the reduction of 4-Nitrophenol. Ultrason Sonochem 44:1–13. https://doi.org/10.1016/j.ultsonch.2018.01.020

Moradi M, Rastakhiz N, Ghaedi M, et al (2020) DFNS/PEI/Cu nanocatalyst for reduction of nitro-aromatic compounds. Catal Lett 151(6):1653–1662. https://doi.org/10.1007/s10562-020-03422-6

Nasrollahzadeh M, Baran T, Sajjadi M et al (2020) Bentonite-supported furfural-based Schiff base palladium nanoparticles: an efficient catalyst in treatment of water/wastewater pollutants. J Mater Sci: Mater Electron 31(15):12856–12871. https://doi.org/10.1007/s10854-020-03839-0

Nemamcha A, Rehspringer JL, Khatmi D (2006) Synthesis of palladium nanoparticles by sonochemical reduction of palladium (II) nitrate in aqueous solution. J Phys Chem B 110(1):383–387. https://doi.org/10.1021/jp0535801

Rahmani F, Haghighi M, Estifaee P (2014) Synthesis and characterization of Pt/Al_2O_3- CeO_2 nanocatalyst used for toluene abatement from waste gas streams at low temperature conventional vs. plasma-ultrasound hybrid synthesis methods. Microporous Mesoporous Mater 185:213–223. https://doi.org/10.1016/j.micromeso.2013.11.019

Riesz P, Kondo T (1992) Free radical formation induced by ultrasound and its biological implications. Free Radical Biol Med 13(3):247–270. https://doi.org/10.1016/0891-5849(92)90021-8

Sun X, He P, Gao Z, Liao Y, Weng S, Zhao Z, Song H, Zhao Z (2019) Multi-crystalline N-doped Cu/Cu_xO/C foam catalyst derived from alkaline N-coordinated HKUST-1/CMC for enhanced 4- nitrophenol reduction. J Colloid Interface Sci 553:1–13. https://doi.org/10.1016/j.jcis.2019.06.004

Tang J, Mu B, Zong L et al (2018) One-step synthesis of magnetic attapulgite/carbon supported NiFe-LDHs by hydrothermal process of spent bleaching earth for pollutants removal. J Clean Prod 172:673–685. https://doi.org/10.1016/j.jclepro.2017.10.181

Vafaeian Y, Haghighi M, Aghamohammadi S (2013) Ultrasound assisted dispersion of different amount of Ni over ZSM-5 used as nanostructured catalyst for hydrogen production via CO2 reforming of methane, Energy Convers. Manage 76:1093–1103. https://doi.org/10.1016/j.enconman.2013.08.010

Veisi H, Ozturk T, Karmakar B et al (2020) In situ decorated Pd NPs on chitosan-encapsulated Fe_3O_4/SiO_2-NH_2 as magnetic catalyst in Suzuki-Miyaura coupling and 4-nitrophenol reduction. Carbohyd Polym 235:115966. https://doi.org/10.1016/j.carbpol.2020.115966

Walker DB, Baumgartner DJ, Gerba CP et al (2019) Surface water pollution[M]//Environmental and Pollution Science. Acad Press 2019:261–292. https://doi.org/10.1016/B978-0-12-814719-1.00016-1

Wang W, Cao G (2007) Synthesis and structural investigation of Pd/Ag bimetallic nanoparticles prepared by the solvothermal method. J Nanopart Res 9(6):1153–1161. https://doi.org/10.1007/s11051-006-9203-5

Wang X, Bai Z, Zhao D, Chai Y, Guo M, Zhang J (2013) New synthetic route to Mg-Al-CO_3 layered double hydroxide using magnesite. Mater Res Bull 48:1228–1232. https://doi.org/10.1016/j.materresbull.2012.11.096

Wang Y, Qiao M, Li YF, Wang SY (2018) Tuning surface electronic configuration of NiFe LDHs nanosheets by introducing cation vacancies (Fe or Ni) as highly efficient electrocatalysts for oxygen evolution reaction. Small 14:1800136. https://doi.org/10.1002/smll.201800136

Wang S, Sun H, Qiao P et al (2021) NiS/Pt nanoparticles co-decorated black mesoporous TiO_2 hollow nanotube assemblies as efficient hydrogen evolution photocatalysts. Appl Mater Today 22:100977. https://doi.org/10.1016/j.apmt.2021.100977

Wu Z, Lin H, Wang Y et al (2016) Enhanced catalytic degradation of 4-NP using a superhydrophilic PVDF membrane decorated with Au nanoparticles[J]. RSC Adv 6(67):62302–62309. https://doi.org/10.1039/C6RA11380J

Wunder S, Polzer F, Lu Y et al (2010) Kinetic analysis of catalytic reduction of 4-nitrophenol by metallic nanoparticles immobilized in spherical polyelectrolyte brushes. J Phys Chem C 114(19):8814–8820. https://doi.org/10.1021/jp101125j

Yin D, Zhang J, Li W, Fu Y (2020) Hyaluronic acid-guided synthesis of Pd nanocatalysts for transfer hydrogenation of 4-nitrophenol. Catal Lett 151(7):1902–1910. https://doi.org/10.1007/s10562-020-03455-x

Zarei M, Seyedi N, Maghsoudi S et al (2020) Green synthesis of Ag nanoparticles on the modified graphene oxide using Capparis spinosa fruit extract for catalytic reduction of organic dyes. Inorg Chem Commun 123(6):108327. https://doi.org/10.1016/j.inoche.2020.108327

Zhang P, Shao C, Zhang Z et al (2011) In situ assembly of well-dispersed Ag nanoparticles (AgNPs) on electrospun carbon nanofibers (CNFs) for catalytic reduction of 4-nitrophenol. Nanoscale 3(8):3357–3363. https://doi.org/10.1039/c1nr10405e

Zhang Y, Yang Q, Li X et al (2020) A Cu (I)–I coordination polymer fluorescent chemosensor with amino-rich sites for nitro aromatic compound (NAC) detection in water. CrystEngComm 22(34):5690–5697. https://doi.org/10.1039/D0CE00835D

Zhao S, Zhu H, Wang H et al (2019) Free-standing graphene oxide membrane with tunable channels for efficient water pollution control. J Hazard Mater 366:659–668. https://doi.org/10.1016/j.jhazmat.2018.12.055

Zhou W, Li W, Wang JQ et al (2014) Ordered mesoporous black TiO_2 as highly efficient hydrogen evolution photocatalyst. J Am Chem Soc 136(26):9280–9283. https://doi.org/10.1021/ja504802q

Zhou D, Cai Z, Jia Y et al (2018) Activating basal plane in NiFe layered double hydroxide by Mn^{2+} doping for efficient and durable oxygen evolution reaction. Nanoscale Horizons 3(5):532–537. https://doi.org/10.1039/C8NH00121A